The Journal of Chemical Physics

A microcanonical approach to temperature-transferable coarse-grained models using the relative entropy

Cite as: J. Chem. Phys. **155**, 094102 (2021); https://doi.org/10.1063/5.0057104
Submitted: 17 May 2021 • Accepted: 10 August 2021 • Published Online: 02 September 2021

Evan Pretti and M. Scott Shell

The Journal of Chemical Physics ARTICLE scitation.org/journal/jcp

A microcanonical approach to temperature-transferable coarse-grained models using the relative entropy

Cite as: J. Chem. Phys. 155, 094102 (2021); doi: 10.1063/5.0057104
Submitted: 17 May 2021 • Accepted: 10 August 2021 •
Published Online: 2 September 2021

Evan Pretti and M. Scott Shell[a)]

AFFILIATIONS

Department of Chemical Engineering, Engineering II Building, University of California, Santa Barbara, Santa Barbara, California 93106-5080, USA

[a)]Author to whom correspondence should be addressed: shell@ucsb.edu

ABSTRACT

Bottom-up coarse-graining methods provide systematic tools for creating simplified models of molecular systems. However, coarse-grained (CG) models produced with such methods frequently fail to accurately reproduce all thermodynamic properties of the reference atomistic systems they seek to model and, moreover, can fail in even more significant ways when used at thermodynamic state points different from the reference conditions. These related problems of representability and transferability limit the usefulness of CG models, especially those of strongly state-dependent systems. In this work, we present a new strategy for creating temperature-transferable CG models using a *single* reference system and temperature. The approach is based on two complementary concepts. First, we switch to a microcanonical basis for formulating CG models, focusing on effective entropy functions rather than energy functions. This allows CG models to naturally represent information about underlying atomistic energy fluctuations, which would otherwise be lost. Such information not only reproduces energy distributions of the reference model but also successfully predicts the correct temperature dependence of the CG interactions, enabling temperature transferability. Second, we show that relative entropy minimization provides a direct and systematic approach to parameterize such classes of temperature-transferable CG models. We calibrate the approach initially using idealized model systems and then demonstrate its ability to create temperature-transferable CG models for several complex molecular liquids.

I. INTRODUCTION

Coarse-graining methods are critically important tools in multiscale modeling, extending the applicability of molecular simulations to complex systems that would otherwise be computationally intractable due to large system sizes or long relaxation timescales.[1–6] In contrast to *ad hoc* top-down coarse-grained (CG) modeling approaches, systematic bottom-up methods for CG modeling—such as iterative Boltzmann inversion (IBI),[7,8] relative entropy minimization,[9–11] and multiscale coarse-graining (MS-CG),[12–15]—create CG models systematically based on reference atomistic simulations within the framework of statistical mechanics. By starting from all-atom (AA) or otherwise detailed simulation data, such methods find effective CG interactions best matching, e.g., configurational probabilities in the case of relative entropy, or forces on CG sites in the case of MS-CG. However, inherent in this systematic simplification is a loss of information about the original model,[9,16,17] leading to inaccurate results when the CG model is applied under conditions differing from the reference AA simulation. Even at the same reference conditions, a CG model faithfully reproducing structural correlations may be unable to accurately capture AA thermodynamic properties.[18–20] Many approaches have now been proposed to ameliorate these *transferability* and *representability* problems, respectively, for various state variables.[21–26]

Here, we consider temperature, in particular, which has been especially challenging to address in CG models. We propose that the nature of the CG model should be rethought in terms of a microcanonical perspective and demonstrate that the relative entropy minimization technique is particularly well-suited to developing models within a microcanonical framework. In turn, we show that it is possible to find temperature-dependent CG models that both capture structure and reproduce AA thermodynamics over a range of temperatures using a single reference trajectory in the coarse-graining procedure.

To discuss how information loss hinders CG models from accurately recovering the behavior of underlying AA systems, we first review some statistical-mechanical results. Consider an AA system of n particles with coordinates $\mathbf{r}^n$ and a potential energy function $U_{\mathrm{AA}}(\mathbf{r}^n)$ in the canonical ensemble with volume V and temperature $T = 1/k_B\beta$. To create a CG system from it, we group particles into $N < n$ sites and define a mapping function $\mathbf{M}(\mathbf{r}^n)$ from AA coordinates to CG coordinates $\mathbf{R}^N$. Of course, we lose information about the original system already after this step as each $\mathbf{R}^N$ has an entire space of $\mathbf{r}^n$ that corresponds to it. Importantly, however, one can exactly capture the projected CG behavior of the equilibrium AA system if the CG model adopts an interaction energy function equal to

$$W_{\mathrm{AA}}(\mathbf{R}^N) = -k_B T \ln\left(V^{N-n} \int e^{-\beta U_{\mathrm{AA}}(\mathbf{r}^n)} \delta\left[\mathbf{R}^N - \mathbf{M}(\mathbf{r}^n)\right] d\mathbf{r}^n\right), \tag{1}$$

the AA potential of mean force (PMF).[9,18,27] However, even for a simple pairwise U_{AA}, the dependence of W_{AA} on $\mathbf{R}^N$ will be complex and not easily decomposable into a pairwise form due to multibody effects.[22,28,29] To make simulations of the final CG model tractable, a pairwise approximate CG potential $W_{\mathrm{CG}}(\mathbf{R}^N)$ is typically employed, and a systematic coarse-graining algorithm then searches for the W_{CG} best matching W_{AA}. (We use the notation W_{CG} in this work for CG interaction potentials, rather than, e.g., U or U_{CG}, to emphasize their connection with an underlying PMF W_{AA}.) As discussed above, the criterion for "best" can use correspondence of forces as in MS-CG, probability distributions $\mathscr{P}_{\mathrm{AA}}(\mathbf{r}^n)$ vs $\mathscr{P}_{\mathrm{CG}}(\mathbf{R}^N)$ as in relative entropy minimization, or low-dimensional structural correlations as in iterative Boltzmann inversion (IBI)[7,8] and inverse Monte Carlo (IMC) coarse-graining.[28,30]

Neglecting multibody effects in the approximation of W_{AA} by W_{CG} can be problematic when transferring CG models from one density to another or between compositions for multicomponent mixtures, as PMFs can be strongly dependent on these state variables.[31,32] A number of techniques have been proposed to tackle these problems using bottom-up CG methods. For example, IBI has been modified to include Kirkwood–Buff theory[33,34] to more accurately coarse-grain liquid mixtures and to use simulations from multiple reference states to improve transferability.[35,36] Extensions of the MS-CG method have been proposed that also support multiple reference states in an extended-ensemble formulation[21,37] as well as three-body[38,39] and density-dependent[40–42] interactions. Local density potentials, which adjust interactions based on the local environments around CG sites,[43] serve as another technique for handling multibody effects. They have been applied successfully with the relative entropy approach to capture phase behavior in highly non-ideal liquid mixtures,[22,44] and similar local density and order parameter-dependent potentials have been used successfully with MS-CG[23,45–47] and other coarse-graining approaches.[48,49]

Temperature remains a critically important thermodynamic variable of concern for CG model transferability. The temperature dependence of effective interactions in fluid systems has widely been investigated[50–55] and has relevance to phase behavior;[56,57] strongly temperature-dependent phenomena are also present in polymer systems, including proteins.[58,59] Yet, correctly capturing temperature dependence can be very difficult, and systematic coarse-graining methods that identify W_{CG} with W_{AA} as a kind of T-independent potential energy can be fundamentally flawed. As can be seen in Eq. (1), W_{AA} has a complex, non-linear dependence on T and, in general, is a temperature-dependent *free energy* for effective CG interactions,[18] with distinct energetic and entropic contributions.[60] Even more broadly, however, a CG interaction W_{CG} that correctly captures the behavior of $W_{\mathrm{AA}}(\mathbf{R}^N)$ will still not alone be capable of recapitulating average AA energies $\langle U_{\mathrm{AA}}\rangle$ or the distribution thereof. For example, it can be shown[26,61] that a systematic discrepancy will occur between $\langle W_{\mathrm{CG}}\rangle$ and $\langle U_{\mathrm{AA}}\rangle$, even without attempting to transfer a CG model to a new temperature.

As with density, several recent approaches have sought to address issues of transferability and representability in the temperature-energy space. A straightforward way to transfer a CG model over a relatively small temperature interval is via reweighting, as has been demonstrated with the MS-CG approach.[24] However, reweighting techniques are ineffective over large temperature ranges due to statistical noise and lack of overlap between energy probability distributions,[62] and it may be impractical to regenerate a CG model for every desired temperature. Furthermore, this method does not solve the problem of representability with respect to AA energies. Recent works by Lebold and Noid[25,26] present a dual-potential approach to modeling AA energies and predicting CG model temperature dependence; creating these models requires a separate optimization step on top of an existing CG model. Another set of methods addressing transferability issues involves models whose CG sites can take on multiple distinct states. These include "surface hopping"[63,64] and an extension of the "ultra-coarse-graining" or UCG methodology[65,66] by Jin, Yu, and Voth[57] to incorporate semi-global density potentials. Finally, although many of these systematic approaches have been proposed, most practically useful temperature-transferable models for solution and polymer systems[58,67–69] rely on *ad hoc* rescaling or linear and non-linear fitting to capture changes in model parameters with temperature. Such models can be sufficient to accurately reproduce the dependence of CG configurational probabilities on temperature. However, if a deeper statistical-mechanical understanding of the temperature dependence of a CG view of a system is sought, it is difficult to extract from these kinds of models.

In the present work, we extend the relative entropy coarse-graining approach[9–11] to provide a systematic and statistical-mechanically consistent way to generate temperature-transferable CG models that also correctly reproduce AA energy distributions over a range of temperatures. In this approach, we first posit that temperature-transferable CG models should be formulated in the microcanonical ensemble. Thus, rather than targeting the temperature-dependent $W_{\mathrm{AA}}(\mathbf{R}^N)$, they should approximate the microcanonical quantity from which it can be generated, $\Omega_{\mathrm{AA}}(E, \mathbf{R}^N) = e^{S_{\mathrm{AA}}(E,\mathbf{R}^N)/k_B}$, which gives the number of AA states mapping onto a given CG configuration with a given energy (related to the entropy in the joint energy-configuration space). The precise relationship is

$$\begin{aligned} e^{-\beta W_{\mathrm{AA}}(\mathbf{R}^N)} &= \int e^{-\beta E} \Omega_{\mathrm{AA}}(E, \mathbf{R}^N)\, dE \\ &= \int e^{-\beta E + S_{\mathrm{AA}}(E,\mathbf{R}^N)/k_B}\, dE. \end{aligned} \tag{2}$$

It is easy to see that this microcanonical formulation explicitly extracts the temperature dependence such that for any β, it is possible to predict the effective CG interaction. Along the same lines, this approach predicts the probability for observing a CG configuration with a given energy as projected from the AA ensemble,

$$\mathscr{P}_{\mathrm{AA}}\left(E,\mathbf{R}^N\right) \propto e^{-\beta E}\Omega_{\mathrm{AA}}\left(E,\mathbf{R}^N\right) = e^{-\beta E+S_{\mathrm{AA}}\left(E,\mathbf{R}^N\right)/k_B}. \tag{3}$$

Here, our core proposal is that temperature-transferable CG models should target the approximation

$$\Omega_{\mathrm{CG}}\left(E,\mathbf{R}^N\right) \approx \Omega_{\mathrm{AA}}\left(E,\mathbf{R}^N\right) \tag{4}$$

rather than $W_{\mathrm{CG}} \approx W_{\mathrm{AA}}$ as has been the conventional basis for bottom-up CG models. Extending the idea of matching probability distributions, CG approximations to $\Omega_{\mathrm{AA}}(E,\mathbf{R}^N)$ can be performed by aligning the AA and CG-predicted joint configuration/energy distributions, where the CG model now gives

$$\mathscr{P}_{\mathrm{CG}}\left(E,\mathbf{R}^N\right) \propto e^{-\beta E}\Omega_{\mathrm{CG}}\left(E,\mathbf{R}^N\right) = e^{-\beta E+S_{\mathrm{CG}}\left(E,\mathbf{R}^N\right)/k_B}. \tag{5}$$

A straightforward approach to this problem is to minimize the relative entropy in this joint space. The conventional definition of the relative entropy measures the overlap of the configurational distributions and is given by

$$S_{\mathrm{rel}} = \int \mathscr{P}_{\mathrm{AA}}\left(\mathbf{R}^N\right)\ln\frac{\mathscr{P}_{\mathrm{AA}}\left(\mathbf{R}^N\right)}{\mathscr{P}_{\mathrm{CG}}\left(\mathbf{R}^N\right)}\,d\mathbf{R}^N, \tag{6}$$

where here the relative entropy compares probability distributions over CG coordinates in the AA and CG models, $\mathscr{P}_{\mathrm{AA}}(\mathbf{R}^N)$ and $\mathscr{P}_{\mathrm{CG}}(\mathbf{R}^N)$. The microcanonical-formulated CG models, which also predict an energy distribution, then suggest that we instead define

$$S^*_{\mathrm{rel}} = \iint \mathscr{P}_{\mathrm{AA}}\left(E,\mathbf{R}^N\right)\ln\frac{\mathscr{P}_{\mathrm{AA}}\left(E,\mathbf{R}^N\right)}{\mathscr{P}_{\mathrm{CG}}\left(E,\mathbf{R}^N\right)}\,dE\,d\mathbf{R}^N, \tag{7}$$

involving joint distributions $\mathscr{P}_{\mathrm{AA}}(E,\mathbf{R}^N)$ and $\mathscr{P}_{\mathrm{CG}}(E,\mathbf{R}^N)$ over CG coordinates along with AA energies. The interpretation of these probabilities is as follows. Each CG configuration $\mathbf{R}^N$ contains a number of AA configurations $\mathbf{r}^n$ that map to it, giving a distribution of AA energies E conditioned on the CG coordinates, $\mathscr{P}_{\mathrm{AA}}(E|\mathbf{R}^N)$. A conventional CG model only attempts to capture $\mathscr{P}_{\mathrm{AA}}(\mathbf{R}^N)$, discarding information about these energy fluctuations that are intimately tied to the temperature dependence of effective interactions between CG sites. In contrast, by attempting to capture the joint distribution, a microcanonical CG model can retain some of this information.

In this work, we show how this microcanonical perspective produces CG force fields that are both temperature-transferable and that predict distributions of expected energies for models based on reference AA systems. This modified method, which minimizes the relative entropy in the space of both energies and configurations to approximate $\Omega_{\mathrm{CG}}(E,\mathbf{R}^N) \approx \Omega_{\mathrm{AA}}(E,\mathbf{R}^N)$, has several benefits in extracting transferability information from reference AA simulations, relative to models not containing information about underlying energy fluctuations. Importantly, it allows for the development of a CG model from a single AA simulation at one temperature, in a single optimization, to produce a thermodynamically consistent temperature-transferable model. In place of single energy values for each CG interaction, these models now provide *distributions* of interaction energies, along with effective interactions (e.g., CG force fields) that can be used in standard molecular simulations. Furthermore, the models can be decomposed in a dual-potential-like manner at any temperature to study the pairwise potentials representing the mean and variance of the energy distributions or, alternatively, the energetic and entropic contributions to the free energy. This decomposition emerges in a straightforward way within the present statistical–mechanical framework.

II. THEORY AND METHODS

Here, we discuss the theoretical details of the microcanonical coarse-graining approach and its implementation with relative entropy optimization. While we summarize the standard relative entropy coarse-graining approach, we omit the details of the numerical optimization and simulation analysis procedures, as these have been described in other works.[9,11,70] Due to the significant number of variables in the theoretical framework, Table I is provided as a guide to the notation used throughout this section.

A. Microcanonical coarse-graining

The present approach centers on the joint distribution over energy and CG coordinates. We can define such a distribution for an AA system as

$$\mathscr{P}_{\mathrm{AA}}\left(E,\mathbf{R}^N\right) = \int \mathscr{P}_{\mathrm{AA}}\left(\mathbf{r}^n\right)\delta\left[E-U_{\mathrm{AA}}\left(\mathbf{r}^n\right)\right]\delta\left[\mathbf{R}^N-\mathbf{M}\left(\mathbf{r}^n\right)\right]d\mathbf{r}^n, \tag{8}$$

where, as discussed previously, $\mathbf{M}(\mathbf{r}^n)$ is a CG mapping, $U_{\mathrm{AA}}(\mathbf{r}^n)$ is the AA force field, and $\mathscr{P}_{\mathrm{AA}}(\mathbf{r}^n) \propto e^{-\beta U_{\mathrm{AA}}(\mathbf{r}^n)}$ is the corresponding canonical configurational probability distribution. It is convenient to define an energy-specific density of states and corresponding entropy

$$\begin{aligned}\Omega_{\mathrm{AA}}\left(E,\mathbf{R}^N\right) &= e^{S_{\mathrm{AA}}\left(E,\mathbf{R}^N\right)/k_B}\\ &= V^{N-n}\int \delta\left[E-U_{\mathrm{AA}}\left(\mathbf{r}^n\right)\right]\delta\left[\mathbf{R}^N-\mathbf{M}\left(\mathbf{r}^n\right)\right]d\mathbf{r}^n\end{aligned} \tag{9}$$

such that it can be shown that

$$\mathscr{P}_{\mathrm{AA}}\left(E,\mathbf{R}^N\right) = \frac{e^{-\beta E}\Omega_{\mathrm{AA}}\left(E,\mathbf{R}^N\right)}{\iint e^{-\beta E'}\Omega_{\mathrm{AA}}\left(E',\mathbf{R}'^N\right)dE'\,d\mathbf{R}'^N} \tag{10}$$

and

$$\mathscr{P}_{\mathrm{AA}}\left(E|\mathbf{R}^N\right) = \frac{e^{-\beta E}\Omega_{\mathrm{AA}}\left(E,\mathbf{R}^N\right)}{\int e^{-\beta E'}\Omega_{\mathrm{AA}}\left(E',\mathbf{R}^N\right)dE'}. \tag{11}$$

The advantage of expressing the joint probability of Eq. (10) in terms of Ω_{AA} is that the temperature dependence is explicitly extracted out. By comparison with Eq. (1), integrating $\mathscr{P}_{\mathrm{AA}}(E,\mathbf{R}^N)$ over energy

TABLE I. Table of symbols used in the description of the microcanonical relative entropy coarse-graining theory.

Symbol	Description	Symbol	Description
$c(R)$, $c_m(\mathbf{R}_m)$	CG term heat capacity	$S_{\mathrm{CG}}(E,\mathbf{R}^N)$	CG microcanonical entropy
E	System energy	S_{rel}	Relative entropy
E_{ij}, E_m	CG term energy	S^*_{rel}	Extended relative entropy
M	Number of CG force field terms	$S_{W_{\mathrm{AA}}}(\mathbf{R}^N)$	AA PMF entropy
$\mathbf{M}(\mathbf{r}^n)$	CG mapping	$\overline{u}(R)$, $\overline{u}_m(\mathbf{R}_m)$	CG term mean energy
n	Number of AA particles	$\overline{U}(\mathbf{R}^N)$	CG mean energy
N	Number of CG sites	$U_{\mathrm{AA}}(\mathbf{r}^n)$	AA potential energy
N_{mol}	Number of molecules	$U_{W_{\mathrm{AA}}}(\mathbf{R}^N)$	AA PMF energy
$\mathscr{P}_{\mathrm{AA}}(E,\mathbf{R}^N)$	AA joint probability	$u_\infty(R)$, $u_{\infty,m}(\mathbf{R}_m)$	CG term reference energy
$\mathscr{P}_{\mathrm{AA}}(E\|\mathbf{R}^N)$	AA conditional probability	$U_\infty(\mathbf{R}^N)$	CG reference energy
$\mathscr{P}_{\mathrm{AA}}(\mathbf{r}^n)$	AA configurational probability	$u_{\infty,1}$	One-body reference energy
$\mathscr{P}_{\mathrm{AA}}(\mathbf{R}^N)$	AA projected probability	$w(R)$, $w_m(\mathbf{R}_m)$	CG term interaction potential
$\mathscr{P}_{\mathrm{CG}}(E,\mathbf{R}^N)$	CG joint probability	$W_{\mathrm{AA}}(\mathbf{R}^N)$	AA PMF for CG coordinates
$\mathscr{P}_{\mathrm{CG}}(E\|\mathbf{R}^N)$	CG conditional probability	$W_{\mathrm{CG}}(\mathbf{R}^N)$	CG force field
$\mathscr{P}_{\mathrm{CG}}(\mathbf{R}^N)$	CG configurational probability	$\gamma(R)$, $\gamma_m(\mathbf{R}_m)$	CG term variance
$\mathscr{P}_m(E_m\|\mathbf{R}_m)$	CG term conditional probability	$\Gamma(\mathbf{R}^N)$	CG variance
R, R_{ij}	CG pair distance	γ_1	One-body variance
$\mathbf{R}_m$	CG term coordinates	$\boldsymbol{\lambda}$	Force field parameters
$\mathbf{r}^n$	AA coordinates	$\boldsymbol{\lambda}_u$	Reference energy parameters
$\mathbf{R}^N$	CG coordinates	$\boldsymbol{\lambda}_\gamma$	Variance parameters
$s(R)$, $s_m(\mathbf{R}_m)$	CG term entropy	$\Omega_{\mathrm{AA}}(E,\mathbf{R}^N)$	AA density of states
$S(\mathbf{R}^N)$	CG entropy	$\Omega_{\mathrm{CG}}(E,\mathbf{R}^N)$	CG density of states
$S_{\mathrm{AA}}(E,\mathbf{R}^N)$	AA microcanonical entropy	$\Omega_m(E_m,\mathbf{R}_m)$	CG term density of states

levels E allows the PMF W_{AA} to be expressed in terms of Ω_{AA},

$$W_{\mathrm{AA}}(\mathbf{R}^N) = -k_BT \ln \int e^{-\beta E}\Omega_{\mathrm{AA}}(E,\mathbf{R}^N)\,dE. \tag{12}$$

This approach separates the parts of W_{AA} involving temperature (the factors of k_BT and $e^{-\beta E}$) from those specific to the system of interest, which are now entirely contained within the temperature-independent function Ω_{AA}. It is interesting to note that, in a microcanonical formulation of dissipative particle dynamics that is conceptually distinct from the approach proposed here, Español and co-workers[71,72] utilized a configuration-dependent entropy with a similar form to that of Eq. (9).

In a conventional CG model optimization with relative entropy, we would minimize Eq. (6) to find $W_{\mathrm{CG}}(\mathbf{R}^N)$, given its chosen functional form with free parameters to be varied for best correspondence with the approximated multibody W_{AA}. This, however, would result in a CG model with unknown temperature dependence and no information about the underlying distribution of AA energies. Instead, in the microcanonical approach using the relative entropy, we minimize Eq. (7) in the joint probability space of both coordinates and energy. The minimization is performed with a CG model defined not by $W_{\mathrm{CG}}(\mathbf{R}^N)$ but instead by an approximate temperature-independent density of states, $\Omega_{\mathrm{CG}}(E,\mathbf{R}^N) = e^{S_{\mathrm{CG}}(E,\mathbf{R}^N)/k_B}$, that best matches the target or "exact" Ω_{AA}. The critical distinction with the conventional approach is that the microcanonical CG formulation becomes inherently temperature-*independent*, while the resulting *effective* CG potential (more correctly, the potential of mean force) becomes a derived function with an explicit temperature dependence,

$$W_{\mathrm{CG}}(\mathbf{R}^N) = -k_BT \ln \int e^{-\beta E}\Omega_{\mathrm{CG}}(E,\mathbf{R}^N)\,dE. \tag{13}$$

Similarly, the CG model now makes a prediction for the distribution of AA energies *within each CG configuration*, that is, the distribution of energies for all AA configurations mapping to a common CG one,

$$\mathscr{P}_{\mathrm{CG}}(E|\mathbf{R}^N) = \frac{e^{-\beta E}\Omega_{\mathrm{CG}}(E,\mathbf{R}^N)}{\int e^{-\beta E'}\Omega_{\mathrm{CG}}(E',\mathbf{R}^N)\,dE'}, \tag{14}$$

as well as the joint configuration-energy distribution,

$$\mathscr{P}_{\mathrm{CG}}(E,\mathbf{R}^N) = \frac{e^{-\beta E}\Omega_{\mathrm{CG}}(E,\mathbf{R}^N)}{\iint e^{-\beta E'}\Omega_{\mathrm{CG}}(E',\mathbf{R}'^N)\,dE'\,d\mathbf{R}'^N}. \tag{15}$$

Using the conditional probability expressions from Eqs. (11) and (14), we can recast the extended relative entropy of Eq. (7) in terms of the conventional relative entropy defined purely in the configuration space and a correction related to the configuration-dependent energy distributions in the two models (see the supplementary material, Sec. II A, for more details),

$$S^*_{\mathrm{rel}} = S_{\mathrm{rel}} + \left\langle \ln \frac{\mathscr{P}_{\mathrm{AA}}\left(E|\mathbf{R}^N\right)}{\mathscr{P}_{\mathrm{CG}}\left(E|\mathbf{R}^N\right)} \right\rangle_{\mathrm{AA}}. \tag{16}$$

Note that here, where E and $\mathbf{R}^N$ appear in AA averages, they denote $U_{\mathrm{AA}}(\mathbf{r}^n)$ and $\mathbf{M}(\mathbf{r}^n)$, respectively. This expression illustrates that the relative entropy incurs an additional penalty (a positive increment) when the energy distributions within CG configurations fail to match beyond the configurational distributions. This formulation also enables existing S_{rel} optimization strategies[11,70] to be extended to the microcanonical approach by attention to the correction term.

B. Approximations to the coarse-grained density of states

To make this formalism practical, we must find a computationally tractable form for Ω_{CG} that approximates the true Ω_{AA}. W_{CG} in a conventional CG model [referred to hereafter as a *non-transferable* model to differentiate from explicitly transferable models following Eq. (13)] is typically cast as a sum of pairwise and other low-body terms. Here, we take Ω_{CG} as a convolution over low-body densities of states to show that this reduces to the same kind of result. Imagine that we decompose the density of states into M distinct "terms." For example, each of these terms might correspond to a distance between a pair of particles (i.e., a pairwise approximation). Then, we would write

$$\Omega_{\mathrm{CG}}\left(E, \mathbf{R}^N\right) = \int \cdots \int \delta\left[E - \sum_{m=1}^{M} E_m\right] \prod_{m=1}^{M} \Omega_m(E_m, \mathbf{R}_m) \times dE_1, \ldots, dE_M, \tag{17}$$

where Ω_m are the densities of states for each of M terms and $\mathbf{R}_m$ each represent some subset of coordinates from $\mathbf{R}^N$ relevant to a particular term $m = 1, \ldots, M$. For a pairwise decomposition, for example, we might have terms such as

$$\Omega_m(E_m, \mathbf{R}_m) = \Omega(E_{ij}, R_{ij}). \tag{18}$$

Equation (17) shows that, within this approximate decomposition, the total density of states is a convolution in energy space over all the component terms. We can show that the effective interaction at a given temperature is, as we would expect, a simple sum of individual term interactions. Substituting Eq. (17) into Eq. (13) and performing the integration over E, we find

$$W_{\mathrm{CG}}\left(\mathbf{R}^N\right) = \sum_{m=1}^{M} w_m(\mathbf{R}_m). \tag{19}$$

Here, the individual CG force interactions w_m stem from a Laplace transform of the corresponding term density of states,

$$w_m(\mathbf{R}_m) = -k_B T \ln \int e^{-\beta E_m} \Omega_m(E_m, \mathbf{R}_m)\, dE_m. \tag{20}$$

We can also define conditional probability distributions for each term,

$$\mathscr{P}_m(E_m|\mathbf{R}_m) = e^{-\beta[E_m - w_m(\mathbf{R}_m)]} \Omega_m(E_m, \mathbf{R}_m) \tag{21}$$

or, alternatively,

$$\mathscr{P}_m(E_m|\mathbf{R}_m) = \frac{e^{-\beta E_m} \Omega_m(E_m, \mathbf{R}_m)}{\int e^{-\beta E'_m} \Omega_m(E'_m, \mathbf{R}_m)\, dE'_m}, \tag{22}$$

and we show that the overall conditional CG energy probability distribution is a convolution of the term distributions,

$$\mathscr{P}_{\mathrm{CG}}\left(E|\mathbf{R}^N\right) = \int \cdots \int \delta\left[E - \sum_{m=1}^{M} E_m\right] \prod_{m=1}^{M} \mathscr{P}_m(E_m|\mathbf{R}_m) \times dE_1, \ldots, dE_M. \tag{23}$$

We see overall that an additive decomposition of the PMF is associated with a termwise decomposition of the density of states, in which energies associated with each term are sampled independently up to the constraint that they sum to the total E.

To make progress, we must propose a particular dependence of each Ω_m on E_m, which, in turn, specifies the dependence of each w_m on T by Eq. (20), and a particular probability distribution family for $\mathscr{P}_m$ and $\mathscr{P}_{\mathrm{CG}}\left(E|\mathbf{R}^N\right)$. We choose a Gaussian functional form for Ω_m, which can be shown to lead to a normal distribution for $\mathscr{P}_m$. This is motivated not only by the central limit theorem (which we might expect to be relevant to high degrees of coarsening with many AA configurations mapping to each CG one) but also by mathematical convenience as the convolution in Eq. (23) then becomes trivial to carry out. Specifically, we take

$$\Omega_m(E_m, \mathbf{R}_m) = \frac{\mathcal{C}_m}{\sqrt{2\pi\gamma_m(\mathbf{R}_m)}} \exp\left(-\frac{[E_m - u_{\infty,m}(\mathbf{R}_m)]^2}{2\gamma_m(\mathbf{R}_m)}\right), \tag{24}$$

where $\mathcal{C}_m$ is an arbitrary normalization constant, which we set equal to 1 in this work as it cancels in Eq. (22) and thus does not affect any of the energy probability distributions (see the supplementary material, Sec. II B, for further discussion of this assignment). Importantly, $u_{\infty,m}(\mathbf{R}_m)$ and $\gamma_m(\mathbf{R}_m)$ are temperature-independent parameters defining the configuration dependence of the term densities of states; if the terms are a pairwise decomposition, for example, we have $u_\infty(R_{ij})$ and $\gamma(R_{ij})$, which could be modeled by splines or tabulated functions. By Eq. (22), we then find the term energy distribution

$$\mathscr{P}_m(E_m|\mathbf{R}_m) = \frac{1}{\sqrt{2\pi\gamma_m(\mathbf{R}_m)}} \exp\left(-\frac{[E_m - \overline{u}_m(\mathbf{R}_m)]^2}{2\gamma_m(\mathbf{R}_m)}\right), \tag{25}$$

where it can be shown with some algebra that the mean energy is

$$\overline{u}_m(\mathbf{R}_m) = u_{\infty,m}(\mathbf{R}_m) - \beta\gamma_m(\mathbf{R}_m). \tag{26}$$

Note that, with $\mathcal{C}_m = 1$, Ω_m takes the exact form of a normal probability density with mean $u_{\infty,m}$, but $\mathscr{P}_m$ is the correct, explicitly temperature-dependent, probability density function for the energy E_m. The notation $u_{\infty,m}$ distinguishes this temperature-independent

reference energy in the density of states from the mean energy $\overline{u}_m$, which tends to $u_{\infty,m}$ in the $T \to \infty$ limit.

Now, by Eq. (20), the effective term free energy takes the form

$$w_m(\mathbf{R}_m) = u_{\infty,m}(\mathbf{R}_m) - \frac{\beta}{2}\gamma_m(\mathbf{R}_m). \tag{27}$$

The entropic component of the term interaction then readily follows:

$$s_m(\mathbf{R}_m) = -\frac{\partial w_m}{\partial T} = -\frac{k_B\beta^2}{2}\gamma_m(\mathbf{R}_m), \tag{28}$$

which, of course, is consistent with the relation

$$\overline{u}_m(\mathbf{R}_m) = w_m(\mathbf{R}_m) + Ts_m(\mathbf{R}_m) = u_{\infty,m}(\mathbf{R}_m) - \beta\gamma_m(\mathbf{R}_m). \tag{29}$$

These equations tie together the energy distribution-centric representation of the system, in which both the reference energies $u_{\infty,m}$ and variances γ_m of the microcanonical representation provide the energy-entropy decomposition of the effective interactions. Finally, we can find a heat capacity contribution,

$$c_m(\mathbf{R}_m) = \frac{\partial \overline{u}_m}{\partial T} = k_B\beta^2\gamma_m(\mathbf{R}_m). \tag{30}$$

The scaling $c_m \sim T^{-2}$ arising naturally from the use of the normal distribution may not be appropriate for all systems, especially when extrapolating over large temperature ranges. However, as we will show, it is still capable of capturing the temperature dependence of configurations and energy distributions for a variety of systems and conditions.

With these results, it becomes straightforward to use Eqs. (23) and (25) to show that the overall energy distribution also has a normal form,

$$\ln \mathscr{P}_{\mathrm{CG}}(E|\mathbf{R}^N) = -\frac{\left[E - \overline{U}(\mathbf{R}^N)\right]^2}{2\Gamma(\mathbf{R}^N)} - \frac{1}{2}\ln\left[2\pi\Gamma(\mathbf{R}^N)\right], \tag{31}$$

where

$$\begin{aligned}
\overline{U}(\mathbf{R}^N) &= U_\infty(\mathbf{R}^N) - \beta\Gamma(\mathbf{R}^N) \\
&= \sum_{m=1}^{M} \overline{u}_m(\mathbf{R}_m), \\
U_\infty(\mathbf{R}^N) &= \sum_{m=1}^{M} u_{\infty,m}(\mathbf{R}_m), \\
\Gamma(\mathbf{R}^N) &= \sum_{m=1}^{M} \gamma_m(\mathbf{R}_m).
\end{aligned} \tag{32}$$

Similarly, Eq. (19) then implies a term-additive overall force field—an approximation to $W_{\mathrm{AA}}(\mathbf{R}^N)$ at *any* temperature—of the form

$$\begin{aligned}
W_{\mathrm{CG}}(\mathbf{R}^N) &= \sum_{m=1}^{M} u_{\infty,m}(\mathbf{R}_m) - \frac{\beta}{2}\sum_{m=1}^{M}\gamma_m(\mathbf{R}_m) \\
&= U_\infty(\mathbf{R}^N) - \frac{\beta}{2}\Gamma(\mathbf{R}^N).
\end{aligned} \tag{33}$$

Note that this can also be written as

$$\begin{aligned}
W_{\mathrm{CG}}(\mathbf{R}^N) &= \sum_{m=1}^{M} \overline{u}_m(\mathbf{R}_m) - T\sum_{m=1}^{M} s_m(\mathbf{R}_m) \\
&= \overline{U}(\mathbf{R}^N) - TS(\mathbf{R}^N),
\end{aligned} \tag{34}$$

where $S(\mathbf{R}^N) = \sum_{m=1}^{M} s_m(\mathbf{R}_m)$. For convenience, we will work from here on with the form given in Eq. (33) since for a given model, there is no hidden temperature dependence within the terms U_∞ and Γ (which are strictly temperature-independent). It is equally valid to work with the energy-entropy representation of Eq. (34), provided that the appropriate temperature dependence of both $\overline{U}$ and S is applied. Equations (26) and (28) can be used to translate between the forms; whatever approach is taken, the relations of Eq. (29) will always hold and the decomposition of the free energy will always remain self-consistent.

We now specialize in the theory, and in the examples to follow, to consider CG models that consist of single-site molecules interacting in a pairwise fashion. In other words, we consider that all M terms correspond to contributions from different pair distances and have the same underlying form of Ω_m. As a result, the effective CG force field becomes

$$W_{\mathrm{CG}}(\mathbf{R}^N) = \sum_{i<j} u_\infty(R_{ij}) - \frac{\beta}{2}\sum_{i<j}\gamma(R_{ij}). \tag{35}$$

This particularly instructive result shows that the microcanonical approach—in conjunction with a pairwise decomposition and Gaussian form of the density of states—admits an effective CG pair interaction that must determine *two* functions, $u_\infty(R)$ and $\gamma(R)$, rather than conventional approaches that target a single interaction potential $w(R)$. In this sense, the decomposition into energetic and entropic terms that govern the temperature dependence of the CG interaction is naturally captured by the microcanonical approach.

It is also important to note that $u_\infty(R)$ and $\gamma(R)$ cannot be separately determined by targeting the configurational distribution at one temperature alone since it is only their combined effect that governs configurational probabilities. However, minimizing the extended relative entropy of Eq. (7), which also includes the effect of the energy distribution per Eq. (31) in which $u_\infty(R)$ and $\gamma(R)$ appear nonlinearly, provides a systematic strategy to determine both of these functions from a single reference system. In practice, we here model these functions as splines, but in general, any functional form would be admissible, and other physically-inspired forms may be more appropriate for particular systems.

Finally, we note that this formalism is not restricted to a strictly pairwise decomposition but is readily extensible to include other common force field forms, including bond, angle, and dihedral interactions. It also accommodates less conventional terms, such as local density potentials, that have been proposed to improve CG model transferability.[22,44,45] In general, any conventional CG force field term can be adapted to the microcanonical coarse-graining approach proposed here by decomposition into temperature-independent and temperature-dependent contributions analogous to Eq. (33).

C. Optimizing temperature-transferable models

The above-discussed approach models the CG force field, W_{CG}, as a pairwise sum involving the pair functions $u_\infty(R)$ and $\gamma(R)$, which here we describe using splines. In the microcanonical approach to coarse-graining, we thus optimize these CG models by minimizing the extended relative entropy S^*_{rel} with respect to the force field parameters, i.e., the spline knots of $u_\infty(R)$ and $\gamma(R)$. This optimization is carried out using a Newton-like algorithm handling linear equality constraints by Gaussian elimination and inequality constraints by projection. The details of the evaluation of the standard S_{rel} and its derivatives are discussed in more detail by Chaimovich and Shell.[11]

Here, we provide a brief overview of the relevant equations for relative entropy minimization that includes information relevant to the optimization of the extended form. We specifically focus on the derivatives of S^*_{rel} that are relevant to gradient-based optimization search methods. Note that in what follows, we assume that the CG models employ the Gaussian form for the density of states as discussed in Sec. II B and consist of pairwise nonbonded interactions between CG sites.

Broadly, if a CG force field is parameterized in terms of a vector of parameters $\boldsymbol{\lambda}$, it can be shown that[9,11]

$$\nabla_{\boldsymbol{\lambda}} S_{\mathrm{rel}} = \beta\langle \nabla_{\boldsymbol{\lambda}} W_{\mathrm{CG}}\rangle_{\mathrm{AA}} - \beta\langle \nabla_{\boldsymbol{\lambda}} W_{\mathrm{CG}}\rangle_{\mathrm{CG}}, \tag{36}$$

where $\langle\cdots\rangle_{\mathrm{AA}}$ and $\langle\cdots\rangle_{\mathrm{CG}}$ represent canonical ensemble averages for the AA and CG systems, respectively. Second derivatives can be found similarly in terms of ensemble averages involving first and second $\boldsymbol{\lambda}$-derivatives of W_{CG}. For extended S^*_{rel}, note that $\mathscr{P}_{\mathrm{AA}}\left(E|\mathbf{R}^N\right)$ is independent of $\boldsymbol{\lambda}$; thus,

$$\nabla_{\boldsymbol{\lambda}} S^*_{\mathrm{rel}} = \nabla_{\boldsymbol{\lambda}} S_{\mathrm{rel}} - \left\langle \nabla_{\boldsymbol{\lambda}} \ln \mathscr{P}_{\mathrm{CG}}\left(E|\mathbf{R}^N\right)\right\rangle_{\mathrm{AA}}. \tag{37}$$

The first term on the RHS of Eq. (37) has been discussed extensively with respect to conventional relative entropy minimization.[9,11,73] For CG models consisting of pairwise nonbonded interactions characterized by spline forms for $u_\infty(R_{ij})$ and $\gamma(R_{ij})$, the to-be-optimized parameters $\boldsymbol{\lambda}_u$ and $\boldsymbol{\lambda}_\gamma$, respectively, are spline knot points. The conventional contribution to the relative entropy derivative following Eq. (36) is implemented for splines as discussed by Chaimovich and Shell,[73] here with $\nabla_{\boldsymbol{\lambda}_u} W_{\mathrm{CG}} = \nabla_{\boldsymbol{\lambda}_u} U_\infty$ and $\nabla_{\boldsymbol{\lambda}_\gamma} W_{\mathrm{CG}} = -(\beta/2)\nabla_{\boldsymbol{\lambda}_\gamma}\Gamma$.

Derivatives of the extended relative entropy that contain the additional term involving the energy distribution according to Eq. (37) then follow

$$\nabla_{\boldsymbol{\lambda}_u} \ln \mathscr{P}_{\mathrm{CG}}\left(E|\mathbf{R}^N\right) = \frac{E - \overline{U}\left(\mathbf{R}^N\right)}{\Gamma\left(\mathbf{R}^N\right)} \nabla_{\boldsymbol{\lambda}_u} U_\infty\left(\mathbf{R}^N\right) \tag{38}$$

and

$$\nabla_{\boldsymbol{\lambda}_\gamma} \ln \mathscr{P}_{\mathrm{CG}}\left(E|\mathbf{R}^N\right) = \left(\frac{1}{2}\left[\frac{E - \overline{U}\left(\mathbf{R}^N\right)}{\Gamma\left(\mathbf{R}^N\right)}\right]^2 - \frac{\beta\left[E - \overline{U}\left(\mathbf{R}^N\right)\right]}{\Gamma\left(\mathbf{R}^N\right)} - \frac{1}{2\Gamma\left(\mathbf{R}^N\right)}\right)\nabla_{\boldsymbol{\lambda}_\gamma}\Gamma\left(\mathbf{R}^N\right). \tag{39}$$

Second derivatives are given in the supplementary material, Sec. II C.

Although this microcanonical coarse-graining formalism with the pairwise approximation as described so far seems reasonable and consistent with other pairwise-based coarse-graining protocols, it likely neglects energy fluctuations not associated with pairwise interactions but rather intra-CG site interactions. Indeed, even when CG sites are non-interacting (i.e., all spatially distanced), energy fluctuations exist due to internal CG-site degrees of freedom. Take the case of an ideal *polyatomic* gas in which each molecule is coarse-grained to a single site. Although there should be no direct pairwise interactions between the CG molecules, the system should still sample a distribution of energies as the internal degrees of freedom of its molecules fluctuate. This suggests the inclusion in the microcanonical formalism of one-body contributions to energy fluctuations that the CG model should capture. In other words, the ideal gas reference case—in which each molecule contributes intramolecular, temperature-dependent mean energies and variances to the overall energy distribution—motivates a more general inclusion of one-body interactions in the microcanonical CG model.

These considerations suggest that we introduce into the CG model additional optimizable parameters $u_{\infty,1}$ and γ_1 that summarize one-body terms in the force field, just as another $(u_{\infty,m}, \gamma_m)$-pair would, but with no configuration dependence. The presence of these parameters does not affect configurational probabilities but allows for the overall energy probability distribution in the CG model to better match the underlying AA system, which would be necessary in the ideal, polyatomic gas limit. This strategy is similar to the energy-matching offset employed by Lebold and Noid[25] in studying implicit solvation models and to the one-body contribution terms used in the state-dependent ultra-coarse-graining approach with rapid local equilibrium (UCG-RLE).[74] However, here, we use two parameters to capture the temperature dependence of this contribution to the mean of the energy distribution and the associated contribution to its fluctuations.

To capture the one-body contributions, we modify the definitions in Eq. (32) to incorporate the net one-body contributions,

$$\begin{aligned} U_\infty\left(\mathbf{R}^N\right) &= N_{\mathrm{mol}} u_{\infty,1} + \sum_{m=1}^{M} u_{\infty,m}(\mathbf{R}_m), \\ \Gamma\left(\mathbf{R}^N\right) &= N_{\mathrm{mol}} \gamma_1 + \sum_{m=1}^{M} \gamma_m(\mathbf{R}_m), \end{aligned} \tag{40}$$

where N_{mol} is the number of molecules in the system. In turn, the influence of these contributions on the gradient of the extended relative entropy is

$$\frac{\partial \ln \mathscr{P}_{\mathrm{CG}}\left(E|\mathbf{R}^N\right)}{\partial(N_{\mathrm{mol}} u_{\infty,1})} = \frac{E - \overline{U}\left(\mathbf{R}^N\right)}{\Gamma\left(\mathbf{R}^N\right)} \tag{41}$$

and

$$\frac{\partial \ln \mathscr{P}_{\mathrm{CG}}\left(E|\mathbf{R}^N\right)}{\partial(N_{\mathrm{mol}} \gamma_1)} = \frac{1}{2}\left[\frac{E - \overline{U}\left(\mathbf{R}^N\right)}{\Gamma\left(\mathbf{R}^N\right)}\right]^2 - \frac{\beta\left[E - \overline{U}\left(\mathbf{R}^N\right)\right]}{\Gamma\left(\mathbf{R}^N\right)} - \frac{1}{2\Gamma\left(\mathbf{R}^N\right)}. \tag{42}$$

Section II C of the supplementary material provides a discussion of second derivatives of $\ln \mathscr{P}_{\mathrm{CG}}\left(E|\mathbf{R}^N\right)$ with respect to these

parameters as well as cross derivatives between them and two-body parameters.

In our implementation of this extended relative entropy optimization problem, a few special adjustments were made on top of the optimization framework discussed in previous works (Refs. 11 and 73). Optimizations of new models either were started with all spline knots set to zero and $u_{\infty,1}$ and γ_1 set to reproduce the mean energy and variance of reference AA simulations or were initialized from models at nearby temperatures as needed to improve numerical convergence. For optimizations of CG models of dodecane and water, spline knots associated with $u_\infty(R)$ and $\gamma(R)$ were constrained to give constant slopes in the inner-core regions of the pairwise potentials—regions that were not well sampled in the simulations and thus have insufficient statistics for determining the corresponding knot values.

D. Molecular dynamics of model fluids

The molecular dynamics (MD) simulations used for AA reference trajectories, CG model optimization, and CG model simulations of ideal harmonic oscillator dimers and tetramers, along with Lennard-Jones/harmonic tetramers, were run using the LAMMPS[75] software package. Simulations were performed with $N_{\text{mol}} = 16$ (ideal) and 256 (Lennard-Jones, LJ) molecules, and Langevin dynamics were performed with time step $\Delta t = 10^{-3}\sigma m^{1/2}\epsilon^{-1/2}$ and time constant $\tau = 0.1\sigma m^{1/2}\epsilon^{-1/2}$ to maintain temperatures at chosen values between $k_BT/\epsilon = 1.2$ and 1.6 for the ideal systems and 1.1 and 1.4 for the LJ systems. Densities were $\rho\sigma^3 = 10^{-3}$ for the ideal systems and 0.8 for the LJ systems. Force constants for harmonic bonds were $\kappa_{\text{AA}} = 10\epsilon\sigma^{-2}$. Simulation results were recorded every 500 steps for between 10^7 and 5×10^7 steps for AA systems or between 10^6 and 5×10^6 steps for CG systems. LJ interactions were truncated and shifted at $r_c = 2.5\sigma$. CG potentials for LJ tetramer systems were represented by cubic splines with a cutoff distance of $R_c = 5.4\sigma$ and with $N_{\text{knot}} = 18$ knot points spaced by $\Delta R_{\text{knot}} = 0.3\sigma$.

Simulations of liquid TraPPE-UA[76] dodecane were performed using the OpenMM[77] software package. We used a time step $\Delta t = 2.5$ fs and an Andersen thermostat with inverse collision frequency $\tau = 250$ fs. $N_{\text{mol}} = 512$ molecules were simulated at temperatures from $T = 350$ to 450 K and at a constant density $\rho = 710$ kg/m^3. Total simulation time at each condition was 25 ns. Similar conditions were employed for the CG optimization simulations with total time 2.5 ns each, although using LAMMPS with a Langevin thermostat. CG potentials were represented by cubic splines with a cutoff distance of $R_c = 2$ nm and $N_{\text{knot}} = 40$, giving $\Delta R_{\text{knot}} = 0.05$ nm. AA simulations of liquid SPC/E[78] and SPC/Fw[79] three-site water were also performed using OpenMM, with time step $\Delta t = 1$ fs, thermostat time $\tau = 100$ fs, and total time 10 ns. $N_{\text{mol}} = 512$ molecules at $\rho = 998$ kg/m^3 for SPC/E and $\rho = 1008$ kg/m^3 for SPC/Fw, and T from 270 to 380 K, were used. CG model-optimization simulations for the water molecules were performed in LAMMPS similarly to dodecane, except with a CG pair potential cutoff distance of $R_c = 1$ nm.

III. COARSE-GRAINING MODEL SYSTEMS

Before applying the extended relative entropy approach with microcanonical coarse-graining to practically relevant systems, we first investigate several idealized but instructive case studies to demonstrate the theoretical framework behind the approach and understand complexities associated with its implementation. We first consider an ideal harmonic oscillator example that can be solved analytically, for comparison with numerical results. We then study the performance of the numerical implementation of the method on a Lennard-Jones tetramer system, demonstrating its ability to predict CG interaction potentials, structure, and energy distributions, before moving on to more realistic fluid models.

A. Ideal harmonic oscillators

Consider an ideal gas of N_{mol} molecules, each a chain of four particles linked by harmonic springs such that the potential energy of the system is

$$U_{\text{AA}}(\mathbf{r}^n) = \frac{\kappa_{\text{AA}}}{2}\sum_{i=1}^{N_{\text{mol}}}\sum_{j=1}^{3}\left|\mathbf{r}_{4i+j-3} - \mathbf{r}_{4i+j-4}\right|^2, \tag{43}$$

where $n = 4N_{\text{mol}}$ and κ_{AA} is the harmonic spring constant. Define a coarse-graining mapping $\mathbf{M}$ such that if $\mathbf{R}^N = \mathbf{M}(\mathbf{r}^n)$, then $\mathbf{R}_k = (\mathbf{r}_{2k-1} + \mathbf{r}_{2k})/2$, where $N = 2N_{\text{mol}}$ [i.e., that lumps together the first two and last two sites within each molecule to form a CG dimer, as shown in Fig. 1(a)]. We begin by finding $\Omega_{\text{AA}}(E, \mathbf{R}^N)$ from its definition in Eq. (9) using the potential of Eq. (43),

$$\begin{aligned}\Omega_{\text{AA}}(E, \mathbf{R}^N) &= \frac{1}{V^{2N_{\text{mol}}}}\int \delta\left[E - \frac{\kappa_{\text{AA}}}{2}\sum_{i=1}^{N_{\text{mol}}}\sum_{j=1}^{3}\left|\mathbf{r}_{4i+j-3} - \mathbf{r}_{4i+j-4}\right|^2\right] \\ &\quad\times \delta\left[\mathbf{R}^N - \mathbf{M}(\mathbf{r}^n)\right] d\mathbf{r}^n.\end{aligned} \tag{44}$$

The required integration over a hypersphere corresponding to the energy constraint on the harmonic potential is complicated by the presence of additional constraints from the CG mapping. Appropriate elimination, diagonalization, and scaling substitutions (see the supplementary material, Sec. II D, for details) yield

$$\begin{aligned}\Omega_{\text{AA}}(E, \mathbf{R}^N) &= \frac{1}{V^{2N_{\text{mol}}}\Gamma(3N_{\text{mol}})}\left(\frac{2\sqrt{6}\pi}{3\kappa_{\text{AA}}}\right)^{3N_{\text{mol}}} \\ &\quad\times \left(E - \frac{\kappa_{\text{AA}}}{3}\sum_{i=1}^{N_{\text{mol}}}\left|\mathbf{R}_{2i} - \mathbf{R}_{2i-1}\right|^2\right)^{3N_{\text{mol}}-1},\end{aligned} \tag{45}$$

where in the context of this example, Γ denotes the gamma function.

With an expression for Ω_{AA}, we can calculate any property related to a hypothetical ideal CG system exactly matching the AA system. From Eq. (12),

$$W_{\text{AA}}(\mathbf{R}^N) = \frac{\kappa_{\text{AA}}}{3}\sum_{i=1}^{N_{\text{mol}}}\left|\mathbf{R}_{2i} - \mathbf{R}_{2i-1}\right|^2 - 3N_{\text{mol}}k_BT\ln\left(\frac{2\sqrt{6}\pi k_BT}{3V^{2/3}\kappa_{\text{AA}}}\right). \tag{46}$$

This result reveals a single harmonic oscillator for each CG molecule (with spring constant $2\kappa_{\text{AA}}/3$) and a separate temperature-dependent but configuration-independent contribution. To

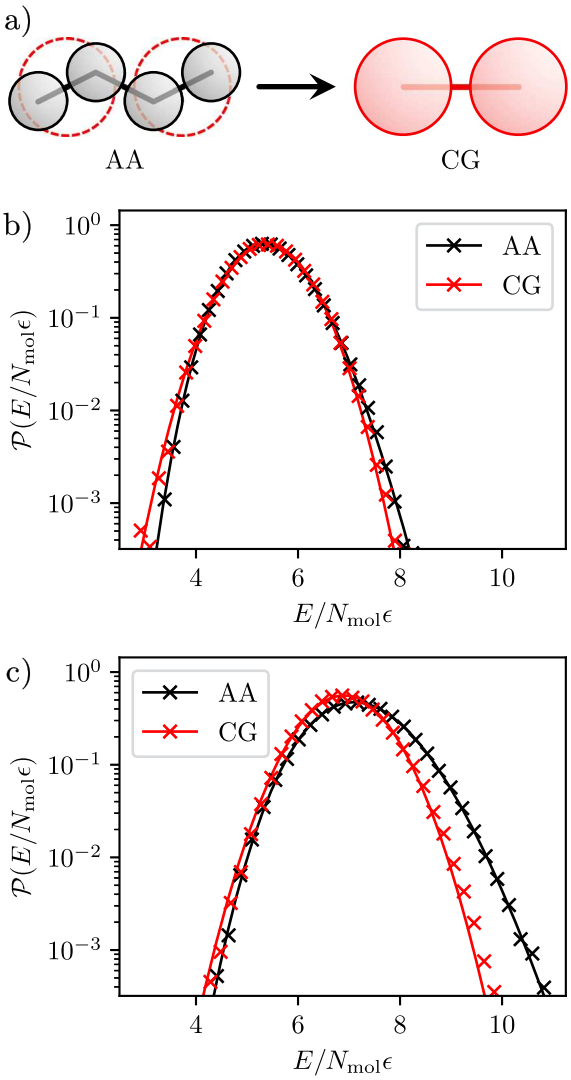

FIG. 1. (a) Coarse-graining a linear tetramer with three harmonic bonds in the AA system to a dimer with one bond in the CG system. (b) Theoretical (–) and simulated (×) AA and CG energy distributions, respectively, for the system with $k_BT/\epsilon = 1.2$. (c) AA results at $k_BT/\epsilon = 1.6$, along with CG results from simulations at $k_BT/\epsilon = 1.6$ using the model optimized at $k_BT/\epsilon = 1.2$.

understand the effect of this latter quantity, we find the configuration-dependent entropy

$$S_{W_{\rm AA}}(\mathbf{R}^N) = -\frac{\partial W_{\rm AA}}{\partial T} = 3N_{\rm mol}k_B\left[1 + \ln\left(\frac{2\sqrt{6\pi}k_BT}{3V^{2/3}\kappa_{\rm AA}}\right)\right] \tag{47}$$

and the configuration-dependent energy

$$\begin{aligned} U_{W_{\rm AA}}(\mathbf{R}^N) &= W_{\rm AA} + TS_{W_{\rm AA}} \\ &= 3N_{\rm mol}k_BT + \frac{\kappa_{\rm AA}}{3}\sum_{i=1}^{N_{\rm mol}}|\mathbf{R}_{2i} - \mathbf{R}_{2i-1}|^2. \end{aligned} \tag{48}$$

The effective energy as a function of CG coordinates consists of a configuration-dependent interaction as well as a temperature-dependent offset that captures the energy contribution of the fluctuating, removed degrees of freedom in the AA system. Note that moving from the AA view of the system with its $3N_{\rm mol}$ oscillators to the CG representation with its $N_{\rm mol}$ oscillators results in a loss of $2N_{\rm mol}$ oscillators; the offset thus contributes $3k_BT/2$ for each of these lost sets of degrees of freedom, as one might expect.

We can also find the conditional energy probability distribution for this CG representation,

$$\mathscr{P}_{\rm AA}(E|\mathbf{R}^N) = \frac{\widetilde{E}^{3N_{\rm mol}-1}e^{-\beta\widetilde{E}}}{(k_BT)^{3N_{\rm mol}}\Gamma(3N_{\rm mol})}, \tag{49}$$

where $\widetilde{E} = E - (\kappa_{\rm AA}/3)\sum_{i=1}^{N_{\rm mol}}|\mathbf{R}_{2i} - \mathbf{R}_{2i-1}|^2$. Equation (49) has the form of a gamma distribution offset by the harmonic energy for the CG system, where the possible energies above this reference energy correspond to different configurations of AA particles consistent with the given CG configuration. While this probability distribution and associated PMF provide an exact CG model for this example system, in general, systems of interest will be much more complicated and an approximate form of $\Omega_{\rm CG}$ will need to be used. To illustrate such an approximation, we use the normal distribution of Sec. II B for the model, corresponding to a CG force field of the form

$$W_{\rm CG}(\mathbf{R}^N) = N_{\rm mol}\left(u_{\infty,1} - \frac{\beta\gamma_1}{2}\right) + \frac{\kappa_{\rm CG}}{2}\sum_{i=1}^{N_{\rm mol}}|\mathbf{R}_{2i} - \mathbf{R}_{2i-1}|^2, \tag{50}$$

along with a conditional energy probability distribution

$$\begin{aligned} \mathscr{P}_{\rm CG}(E|\mathbf{R}^N) = &\frac{1}{\sqrt{2\pi N_{\rm mol}\gamma_1}} \\ &\times \exp\left(-\frac{\left[E + \beta N_{\rm mol}\gamma_1/2 - W_{\rm CG}(\mathbf{R}^N)\right]^2}{2N_{\rm mol}\gamma_1}\right). \end{aligned} \tag{51}$$

It can be shown that the choices $u_{\infty,1} = 6k_BT_0$, $\gamma_1 = 3k_B^2T_0^2$, and $\kappa_{\rm CG} = 2\kappa_{\rm AA}/3$ correspond to the minimum of the relative entropy $S^*_{\rm rel}$, where T_0 is a reference temperature at which the model is parameterized (see the supplementary material, Sec. II D, for more details).

A few things should be noted about the CG model defined by Eqs. (50) and (51). First, the volume dependence appearing in the logarithmic terms present in Eqs. (46) and (47) is absent from $W_{\rm CG}$, as it does not influence the configurational or energy probability distributions relevant to the CG model. A temperature-dependent but configuration-independent contribution is still present; here, $N_{\rm mol}(u_{\infty,1} - \beta\gamma_1/2)$ with $u_{\infty,1} = 6k_BT_0$ and $\gamma_1 = 3k_B^2T_0^2$. This solution turns out to ensure that the mean and variance of the normally distributed $\mathscr{P}_{\rm CG}(E|\mathbf{R}^N)$ match that of the gamma distributed $\mathscr{P}_{\rm AA}(E|\mathbf{R}^N)$ at the reference temperature T_0. The distributions match exactly at $T = T_0$ in the $N_{\rm mol} \to \infty$ limit where the shape of the gamma distribution approaches that of a normal one. However, they diverge as T moves further away from T_0, as the constant heat capacity of the harmonic oscillator model leads to a variance increasing with temperature, while the normal distribution model instead has a constant variance.

The correspondence between the distributions is shown in Fig. 1(b). The exact distribution of AA energies here is found from the original force field $U_{\mathrm{AA}}(\mathbf{r}^n)$ or by integrating $\mathscr{P}_{\mathrm{AA}}(E|\mathbf{R}^N)\mathscr{P}_{\mathrm{AA}}(\mathbf{R}^N)$ over all $\mathbf{R}^N$. In any case, it also follows a gamma distribution,

$$\mathscr{P}_{\mathrm{AA}}(E) = \frac{E^{9N_{\mathrm{mol}}/2-1}e^{-\beta E}}{(k_BT)^{9N_{\mathrm{mol}}/2}\Gamma(9N_{\mathrm{mol}}/2)}. \tag{52}$$

Likewise, integrating the product of Eq. (51) with $\mathscr{P}_{\mathrm{CG}}(\mathbf{R}^N)$ over all position coordinates gives a normal distribution $\mathscr{P}_{\mathrm{CG}}(E)$, with

$$\langle E\rangle_{\mathrm{CG}} = \left(6 - \frac{3T_0}{T}\right)N_{\mathrm{mol}}k_BT_0 + \frac{3N_{\mathrm{mol}}k_BT}{2}, \tag{53}$$

$$\langle E^2\rangle_{\mathrm{CG}} - \langle E\rangle^2_{\mathrm{CG}} = 3N_{\mathrm{mol}}k_B^2T_0^2 + \frac{3N_{\mathrm{mol}}k_B^2T^2}{2}. \tag{54}$$

Both the exact and CG analytical energy distributions (solid lines in Fig. 1) show excellent agreement at $k_BT_0/\epsilon = 1.2$ since choosing $T = T_0$ in Eqs. (52)–(54) gives consistent means $9N_{\mathrm{mol}}k_BT/2$ and variances $9N_{\mathrm{mol}}k_B^2T^2/2$. The black crosses show results from explicit MD simulations of the AA system, while the red crosses stem from random sampling of the distribution of Eq. (51) using an MD trajectory from the CG system. Note that the parameters $u_{\infty,1}$, γ_1, and κ_{CG} in these CG simulations are not set to their analytically optimal values; instead, the employed values are determined by numerically minimizing S^*_{rel} with the help of the derivatives in Eqs. (37)–(39).

Figure 1(c) shows similar results, but this time at a new target temperature of $k_BT/\epsilon = 1.6$. The theoretical and simulated AA distributions are found normally, while the theoretical CG distribution is found using parameters calculated at the original T_0 but extrapolated to the new target T per the temperature-transferable scheme. Likewise, CG simulations are performed at T, but the input parameters are those from optimization at T_0 such that those same parameters are used in the random sampling from the conditional energy probability distribution. Since the exact harmonic oscillator model predicts a mean energy and variance increasing in temperature, while the normal approximation produces a constant variance and a heat capacity decreasing with temperature, the results are as expected. The energy distribution predicted from the CG model has both a lower mean and a variance than the underlying AA system at the new temperature. However, the optimized parameters perform as well as they can to replicate the energy distribution given the constraints of the normal approximation and still provide a good estimate over a range around the parameterization temperature with no training to the AA system at other temperatures.

B. Lennard-Jones tetramers

Having demonstrated the microcanonical coarse-graining approach with an analytical example, we turn to a more complicated case, here a system of linear tetramers each held together by harmonic bonds. We now let nonbonded pairs of particles interact with the Lennard-Jones (LJ) potential $u(r) = 4\epsilon(\sigma^{12}/r^{12} - \sigma^6/r^6)$. We then study the temperature-transferable framework for CG models that coarsen each molecule to a single site. All pairs of CG sites interact with a pairwise potential $w(R)$ composed of a reference energy term $u_\infty(R)$ and a fluctuation term $\gamma(R)$; these terms are represented by splines, as discussed in Sec. II C. This system cannot be treated analytically to create a benchmark against which to compare CG model results; however, the models are readily tested against AA simulations at different temperatures to evaluate the captured temperature dependence.

We begin by considering the accuracy with which the microcanonical CG model recovers pair potentials at various temperatures. A naïve approach to a transferable model might involve linear or nonlinear interpolation of potential parameters using CG models developed at multiple temperatures. In the present formulation, however, a model should be able to achieve similar performance over some temperature range using only a single AA simulation at one reference temperature. We demonstrate this approach for the tetramer system in Fig. 2(a). As controls, we determine two potentials with standard relative entropy optimization at $k_BT/\epsilon = 1.1$ and

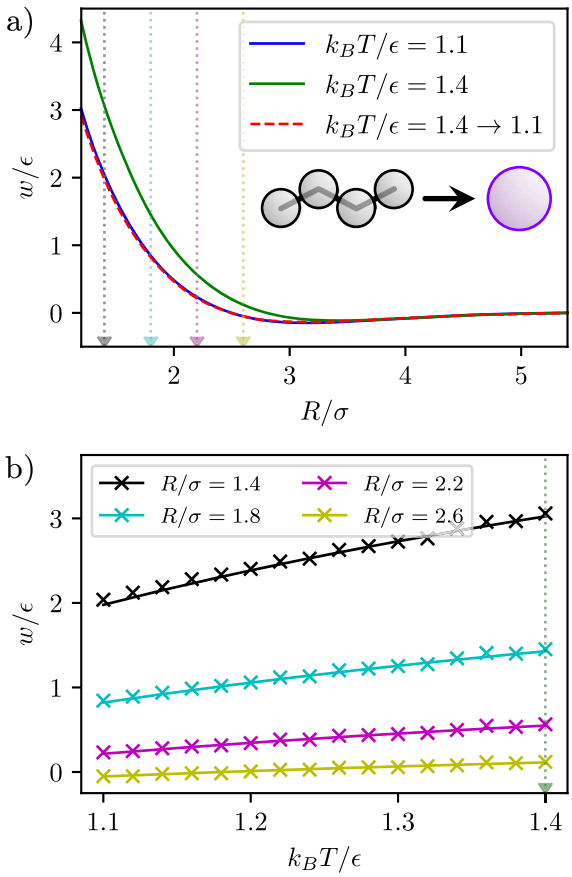

FIG. 2. (a) CG potentials for Lennard-Jones tetramers at density $\rho\sigma^3 = 0.8$, including two potentials found from the ordinary relative entropy approach at $k_BT/\epsilon = 1.1$ and 1.4 and one potential for $k_BT/\epsilon = 1.1$ calculated from a transferable model optimized at $k_BT/\epsilon = 1.4$. (b) Values of CG potentials at particular locations [see the dotted lines in (a)] over a range of temperatures. The crosses are results from independent non-transferable CG models, while the solid lines represent a single transferable model optimized at $k_BT/\epsilon = 1.4$.

$k_BT/\epsilon = 1.4$. Then, we optimize a transferable model at $k_BT/\epsilon = 1.4$ and evaluate its predicted behavior at the two temperatures. The transferable model agrees nearly exactly with the non-transferable model at the parameterization temperature but, more importantly, completely predicts the explicitly determined potential at the lower temperature when extrapolated. Figure S1(a) (see the supplementary material, Sec. I, for all supplementary figures) presents similar results for transfer in the opposite direction in temperature, also showing accurate reproduction of the interaction at the higher temperature when developed at the lower one.

The ability to extrapolate in temperature using the micro-canonical approach is particularly evident in Fig. 2(b), which shows values of CG potentials at select pair separation distances for the temperature-transferable model (optimized at a single temperature from a single reference simulation), in comparison to the same results from non-transferable models optimized independently at each temperature. As seen, the potential values at all the temperatures in the range are predicted well by the transferable model, with a greatly reduced computational effort compared to that required to separately optimize a suite of non-transferable CG models. (In this case, optimization of transferable models required roughly the same number of optimization steps as non-transferable models while taking ~ 60% more computation time due to additional averaging required from Eq. (37). For this particular problem, this is still a major improvement, given the number of temperatures at which models were optimized and that additional AA simulations must be performed to parameterize non-transferable models at new temperatures. In general, performance of transferable vs non-transferable model optimization for other systems was similar.) Figure S1(b) also illustrates the behavior for transfer in the opposite direction starting from $k_BT/\epsilon = 1.1$.

It is important to note the nature of the normal energy approximation used here and its consequences for parameterizing models at different temperatures. Figures S1(c) and S1(d) show values of the nominally temperature-independent reference energy and fluctuation pairwise potentials $u_\infty(R)$ and $\gamma(R)$ at the two parameterization temperature extremes considered in this system. Although similar, the results are distinct at the two endpoints of the temperature range. This is simply a consequence of the approximations taken by the models: were they able to capture the exact dependence of the temperature-independent $\Omega_{\mathrm{AA}}(E, \mathbf{R}^N)$, they would naturally be identical at both temperatures. However, as they represent only local approximations to this density of states for energies and configurations sampled near the parameterization temperature, they will necessarily show differences as this temperature is changed.

As seen in Figs. 2 and S1(b), slight differences in transferability performance occur with the direction taken, with transfer *up* in temperature appearing slightly less accurate than the transfer *down*. However, recall that minimizing S^*_{rel} as defined in Eq. (7) tries to match the overall joint probability distribution $\mathscr{P}(E, \mathbf{R}^N)$ between the AA and CG systems, not just $\mathscr{P}(\mathbf{R}^N)$ as is the case for conventional S_{rel} minimization. The latter approach should, in principle, produce a CG potential that exactly matches the radial distribution function (RDF) $g(R)$ between the systems,[11] and by Henderson's theorem,[80] it will yield a particular interaction potential $w(R)$ unique to that $g(R)$. However, as pointed out by Wang, Stillinger, and Torquato,[81] $g(R)$ may be very insensitive to $w(R)$ for certain systems, i.e., $w(R)$ may be very sensitive to small changes in $g(R)$. Thus, even a small sacrifice in the accuracy at which $g(R)$ is captured in order to better represent the joint configurational and energy distribution could lead to a considerable change in $w(R)$. As such, evaluating a transferable model based on its reproduction of a particular pair potential alone is not very informative with respect to how well it can predict structure and energies.

Therefore, we consider RDFs generated from MD simulations of the transferable CG models across temperature. We quantify the agreement of RDFs from transferable models at particular temperatures, $g(R)$, with those from AA simulations at the same temperatures, $g_{\mathrm{ref}}(R)$, by introducing a distance metric functional

$$D[g, g_{\mathrm{ref}}] = 4\pi\rho \int_0^{R_c} R^2 [g(R) - g_{\mathrm{ref}}(R)]^2 \, dR. \tag{55}$$

To assess their structural accuracy, we compare D for the transferable models to D for non-transferable ones at the same reference temperatures. An example akin to that of Fig. 2(a) is shown in Fig. 3(a), now with $g(R)$ rather than $w(R)$. In this case, the

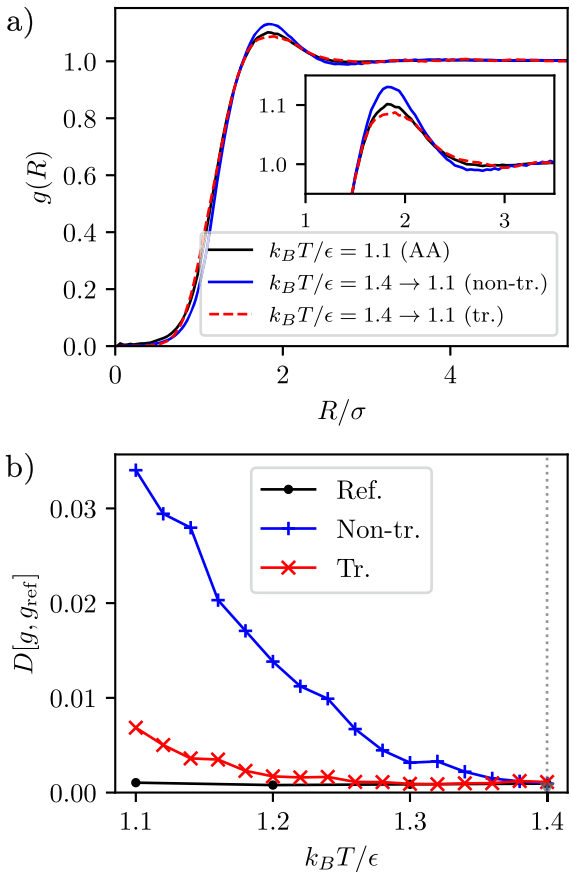

FIG. 3. (a) Radial distribution function for the AA LJ tetramer system at $k_BT/\epsilon = 1.1$, compared with those for transferable (tr.) and non-transferable (non-tr.) CG models parameterized at $k_BT/\epsilon = 1.4$. (b) RDF similarity for models parameterized at $k_BT/\epsilon = 1.4$. The reference (ref.) points give D for a non-transferable CG model optimized individually at each temperature; these are non-zero only due to sampling noise from the finite-length simulations.

potential generated by the fully optimized transferable model from $k_BT/\epsilon = 1.4$ is better able to reproduce the target $g(R)$ at the desired temperature $k_BT/\epsilon = 1.1$ than a non-transferable model optimized at $k_BT/\epsilon = 1.4$. Figure 3(b) then presents the similarity metric D for different temperatures. As the temperature falls from the reference parameterization temperature $k_BT/\epsilon = 1.4$, values of D rise, indicating an increasing deviation of RDFs predicted by the transferable models from the true $g(R)$. Given the linear approximation in β made for the temperature dependence of the potentials, imperfect prediction is to be expected. However, it is encouraging to see that the transferable model significantly outperforms a non-transferable one also parameterized at $k_BT/\epsilon = 1.4$.

Additional plots of D vs T for this system are shown in Fig. S2 using different model-optimization temperatures. Curiously, values of D, representing structural transferability error, are slightly lower in the increasing temperature ($k_BT/\epsilon = 1.1 \rightarrow 1.4$) than the decreasing temperature ($1.4 \rightarrow 1.1$) case, in contrast to the trend in effective potentials implied by Figs. 2(a) and S1(a). The reason for this asymmetry is not clear, although it may be related to the sharpening of the peak of $g(R)$ when moving from higher to lower temperatures vs its broadening when moving in the opposite direction. In any case, these behaviors represent extremal cases, and normally, it would make sense to choose an intermediate temperature during CG model parameterization to provide better structural transferability performance over the desired range of temperature. This intermediate case is also demonstrated in Fig. S2.

To conclude the investigation of this system, we consider how well the transferable models predict energy distributions across temperature space. Properly capturing $\mathscr{P}_{\mathrm{AA}}(E)$ at the parameterization temperature is a representability-related issue that, as we shortly show, even a non-transferable CG model will fail to do, in general. Predicting this distribution at other temperatures is moreover a transferability problem. An ideal CG model developed at a single temperature would address both of these requirements over a range of transferred temperatures. The actual models that we consider here, as a consequence of the approximations made to implement the microcanonical coarse-graining framework, necessarily limit the accuracy to some degree.

Specifically, we discuss the ability of transferable CG models for this system to capture $\mathscr{P}_{\mathrm{AA}}(E)$. Figure 4(a) gives a comparison of different energy distributions predicted by CG models both optimized and evaluated at $k_BT/\epsilon = 1.4$. The black curve gives the target distribution from the AA system, that of U_{AA}, which a perfect transferable model should be able to match exactly. A conventional, non-transferable model yields effective CG energies distributed as indicated by the purple curve labeled $W_{\mathrm{CG,non\text{-}tr}}$, which are only given for comparison as this distribution corresponds to effective configurational free energies, not potential energies. The positive values of $W_{\mathrm{CG,non\text{-}tr}}$ are consistent with the mostly repulsive interactions between sites in the CG model. On the other hand, the transferable model has W_{CG} distributed as illustrated by the green curve ($W_{\mathrm{CG,tr}}$), which while closer to the target distribution due to the constant offset from the one-body terms still represents an effective free energy distribution and thus naturally does not match the AA energies. Section II B discusses why the CG configurational potential at a given temperature is different from the one that should be used to estimate AA energies. Note that the large offset between the means of these distributions is to be expected; this comes entirely from the one-body terms that are absent in the non-transferable model. The pairwise interaction potentials of these two models are effectively identical, and the configurational probability distributions are not influenced by configuration-independent constant offsets, such as the offset applied by the one-body terms.

In contrast, the transferable model inherently makes a prediction for the actual underlying *potential* energies of the AA system. In Fig. 4(a), the blue curve giving the distribution of the function $\overline{U}(\mathbf{R}^N)$ matches the expected mean energy of the target AA system. Here, it is important to note that $\overline{U}(\mathbf{R}^N)$ represents the mean energy of all AA configurations mapping to the same CG one; thus, it is in effect "pre-averaged" over AA configurations within CG states, which is why its distribution is narrow. On the other hand, the CG model can also give the full AA energy distribution by convolving the within-CG-state distribution $\mathscr{P}_{\mathrm{CG}}(E|\mathbf{R}^N)$ with correct sampling of $\mathscr{P}_{\mathrm{CG}}(\mathbf{R}^N)$. That is, a mean and variance can be found for every frame in a CG trajectory, and the resulting collection of normal distributions can be sampled to obtain a final distribution E (dashed red curve) predicting that of U_{AA} almost perfectly as illustrated.

Now, we turn to the energy distributions when the analysis is at a new temperature $k_BT/\epsilon = 1.1$, distinct from the parameterization temperature. Figure 4(b) shows the corresponding results for this temperature-transferred case. The distributions of the W_{CG} are

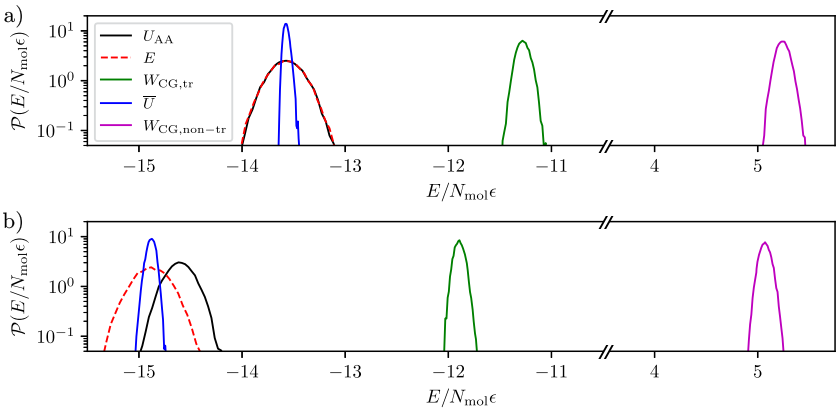

FIG. 4. (a) Energy probability distributions for the LJ tetramer system at $k_BT/\epsilon = 1.4$. $W_{\mathrm{CG,non\text{-}tr}}$ is $W_{\mathrm{CG}}(\mathbf{R}^N)$ for a non-transferable model, while the other distributions including $W_{\mathrm{CG,tr}}$ are from a transferable model. (b) Distributions for the same model as in (a), now simulated at $k_BT/\epsilon = 1.1$.

still far from the AA energy distribution at this new temperature, as expected. There is now a noticeable difference between the expected distribution for U_{AA} and that of E predicted by the temperature-transferable model, although by comparison with Fig. 4(a), the new prediction at the lower temperature is a much better estimate of the new target distribution than the original prediction at the higher temperature. Even if the magnitude of the distribution shift is not recovered exactly, the model correctly captures that $\langle U_{AA}\rangle$ decreases with T, addressing the combined representability and transferability problems associated with reproducing this distribution.

One important issue that needs to be considered is the best method for handling the one-body parameters, $u_{\infty,1}$ and γ_1. Ideally, they would be optimized simultaneously with the rest of the parameters defining the transferable force field, using Eqs. (41) and (42), which is the main approach that we use here. However, in a number of cases, in practice, we found that the precise distribution of AA energy fluctuations between the one-body contribution γ_1 and the two-body term $\gamma(R)$ has a very weak effect on the extended relative entropy. The flexibility in balancing these contributions can lead to amplification of numerical noise in the optimized values of the fluctuations and even failure of the optimization algorithm due to the large condition number of the Hessian of the relative entropy (see Fig. S3 for details). One can simply fix the one-body parameters, setting $N_{\mathrm{mol}}(u_{\infty,1} - \beta\gamma_1)$ and $N_{\mathrm{mol}}\gamma_1$ equal to the mean and variance, respectively, of the energy in an AA trajectory at the reference temperature. They can also be set to zero, or to recapitulate only intramolecular mean energies and variances, using energies taken from a simulation of a single molecule in an infinite volume (i.e., from the ideal gas state). We investigate these choices in more detail in the supplementary material, Sec. II E. However, in general, for the models presented here, we successfully perform optimizations of all parameters simultaneously using well-chosen initial guesses (e.g., from results at nearby temperatures).

IV. APPLICATION TO MOLECULAR FLUIDS

Having explored the microcanonical strategy for coarse-graining the model systems of Sec. III, we turn now to two illustrative and more realistic test cases. For these, we report on results for the strategy involving simultaneous optimization of the one-body terms with the other parameters, as mentioned just above, which produces the best transferability performance.

A. United-atom dodecane

Figure 5 presents results for a CG model of TraPPE united-atom (UA) dodecane, in which each 12-site molecule is coarsened to a single site. Figure 5(a) shows non-transferable CG model potentials at two temperatures 350 and 450 K for a liquid at ρ = 710 kg/m^3 and demonstrates that a third, transferable potential parameterized from the high temperature shows excellent agreement when transferred to the lower one. We see similar accuracy when transferring in the opposite direction [see Figs. S5(a) and S5(b)]. Figure 5(b) quantifies RDF similarity measured for a model optimized at 450 K and used at lower temperatures. The values of D in blue are for a non-transferable model (i.e., the same pair interaction potential at all temperatures), while those in red are for a transferable one. We see good transferability for temperatures close to the optimization conditions, but the transferable model performs less accurately with increased extrapolation downward as one might expect, although still significantly outperforming the non-transferable model.

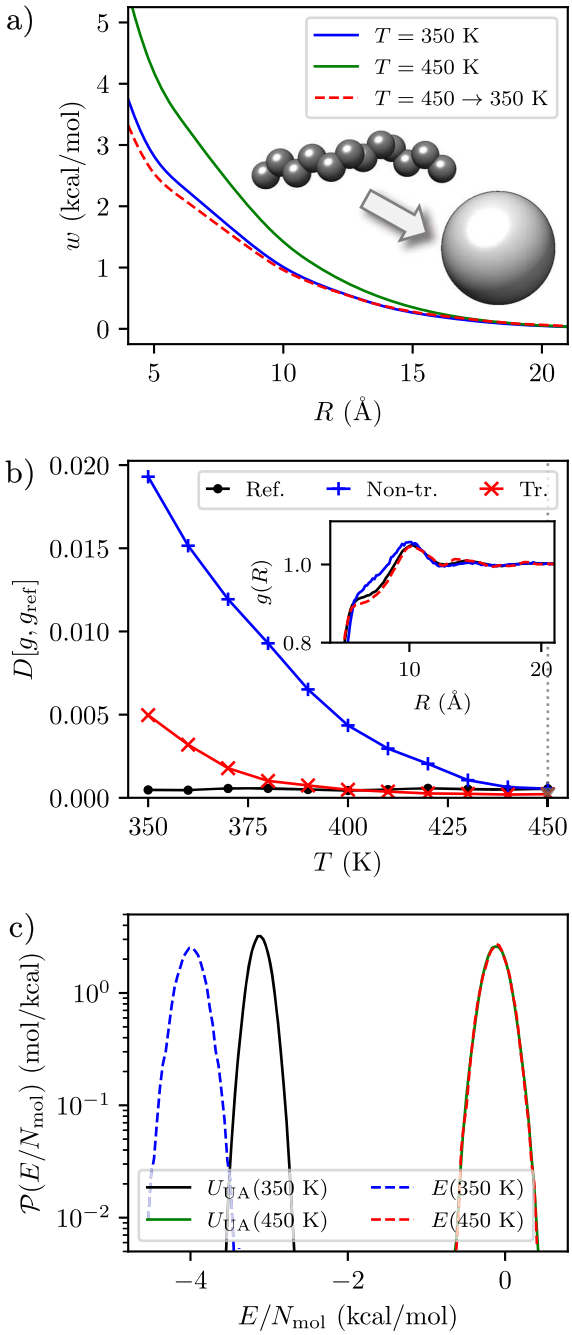

FIG. 5. (a) Transferable CG potentials for TraPPE-UA dodecane between 350 and 450 K. (b) RDF similarity vs temperature for non-transferable (non-tr.) and transferable (tr.) models optimized at 450 K. The inset shows RDFs of the models at 350 K. (c) Predicted CG (E) vs UA (U_{UA}) energy distributions for the transferable model.

The inset in Fig. 5(b) compares UA RDFs of molecular centers of mass at 350 K (black) with CG RDFs at 350 K from non-transferable (blue) and transferable (red) models optimized at 450 K. Along most of the inner "shoulder" region of the RDFs below 10 Å, the transferable model RDF follows the UA result more closely than that of the non-transferable model. Models optimized at 350 K also show good structural transferability performance when extrapolating up in temperature [see Figs. S5(c) and S5(d)]. Finally, as for the Lennard-Jones systems, we show at these two temperature extremes the values of the underlying potentials $u_\infty(R)$ and $\gamma(R)$ in Figs. S5(e) and S5(f). As mentioned before, some differences are seen, highlighting that the transferability performance will be imperfect due to the approximations taken. We note again, however, that for practical use of these transferable models, it may be better to take an intermediate temperature within the range of interest rather than an endpoint, as this will increase the overall transferability accuracy of the models.

Finally, Fig. 5(c) shows predicted energy distributions at two temperatures, 350 and 450 K from the transferable CG model optimized at 450 K, compared to corresponding UA distributions. The energy distribution is captured perfectly at the optimization temperature, just as in the LJ tetramer case. The qualitative decrease in the mean energy with decreasing temperature is also predicted correctly, although the exact magnitude is slightly in error. The discrepancy arises from the approximation of the constant variance made by the chosen model (due to the normal distribution assumption), leading to an effective increase in heat capacity with decreasing temperature. A more appropriate approximation might invoke a constant heat capacity (or one increasing with temperature), but this could come at the loss of simplicity and mathematical tractability of the functional form of $\Omega_m(E_m, \mathbf{R}_m)$. Once again, E from the transferable model at the new temperature gives a more accurate prediction of the behavior of U_{UA} at this temperature than either distribution at the initial temperature.

B. Three-site water models

Finally, we consider a CG model of SPC/E water at a density of 998 kg/m^3 and temperatures within the liquid range. Figure 6 presents results for this model, starting in Fig. 6(a) with CG potentials at 270 and 380 K. Typical single site, pair spline CG models of water show a characteristic functional form,[12,73,82–88] with a strongly T-dependent inner potential well near 3 Å and a variable outer well near 5 Å. We see those same features here but notice unusual behavior of the transferable CG model in its temperature variation. In the outer well, $w(R)$ at 270 K is slightly lower than at 380 K, and the transferable model optimized at 380 K predicts this decrease at 270 K, as expected. However, for the inner well, while the non-transferable CG potential for this system increases when moving from 380 to 270 K, the transferable prediction shows a decrease, moving in the opposite direction from the higher temperature case. Although it may appear that this is a failure of the model, closer examination shows that the slope of the transferred potential, which is related to the effective pair forces, is preserved well particularly around the inner well. We show this more explicitly in Fig. S6, for this case, as well as for the reverse transfer from 270 to 380 K; recovery of the correct forces at this inner well is good in both directions even though significant differences

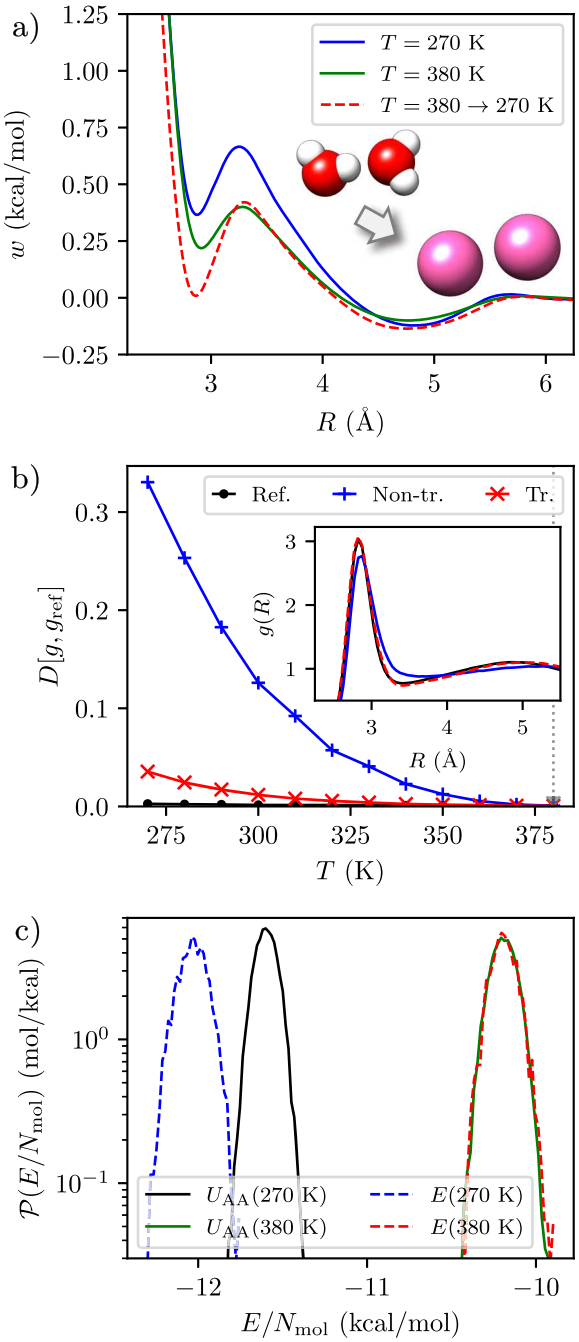

FIG. 6. (a) Transferable CG potentials for SPC/E water between 270 and 380 K. (b) RDF similarity vs temperature for non-transferable (non-tr.) and transferable (tr.) models optimized at 380 K. (c) Predicted CG vs AA energy distributions.

are seen in the potentials $u_\infty(R)$ and $\gamma(R)$ [see Figs. S7(a) and S7(b)].

Interestingly, and relatedly, the transferable model nonetheless exhibits very accurate transferability performance in terms of $g(R)$,

as shown in Fig. 6(b). Although the CG potential transferred from 380 to 270 K has a very different predicted form than that from the non-transferable model optimized directly at 270 K, the transferred potential still very accurately predicts the behavior of $g(R)$ near its first peak and trough. The results from the CG potential transferred from 380 to 270 K are in very close agreement with the AA results, while results from a non-transferable model optimized at 380 K show substantial deviations. Evidently, matching the forces between water molecules near this first peak just below 3 Å is much more important for resolving the temperature dependence than matching the exact potential values. Moreover, the transferable model still does a reasonable job in reproducing AA energy distributions. As shown in Fig. 6(c), it gives a perfect match in mean and variance at the model-optimization temperature 380 K. Transferability of this predicted energy distribution, while not perfect, is still reasonable, as shown at 270 K.

Why then does the transferable model predict changes to the effective $w(R)$ that are so different from explicit, conventional non-transferable CG model optimization at the two temperatures? We hypothesize that this apparent behavior is due to compromises that relative entropy optimization makes, given the approximations made in the microcanonical CG formulation. Specifically, by assuming a normal underlying density of states, Eq. (27) shows that the effective pair interaction $w(R)$ must decrease with increasing β and hence decreasing T. Thus, the non-transferable model in which $w(R)$ increases at lower temperatures would not be possible in the microcanonical case with positive energy variance $\gamma(R)$. To compensate for this limitation, relative entropy minimization attempts to find $w(R)$ that most closely matches the joint probability distribution of configurations and energies in the AA model. As discussed above, it likely leverages the fact that many low-dimensional correlation functions such as $g(R)$ can be insensitive to certain features of the interactions, including longer-range attractions, in contrast to short-range repulsions that tend to be very important.[81,89] This picture is reinforced by the fact that the transferable potential does a good job of reproducing forces rather than absolute pair energies (which interestingly is an idea reinforced in force-matching strategies for coarse-graining[12,90] that seek to recover gradients of the AA PMF). However, we note that other approximations may be relevant to this picture, including the use of low-order CG interactions to capture the complex multi-body AA PMF that is fundamentally of interest. More specifically, here, the low-body decomposition of the energy- and conformation-dependent coarse-projected AA density of states also incurs its own errors, in addition to the assumed form of the density of states.

To gain more insight into the behavior of our water models, we make a comparison with the work of Lebold and Noid[26] in which a dual-potential approach is used to develop single-site CG models for SPC/E water. In particular, Fig. S7(c) corresponds to Fig. 2 of Ref. 26, showing a pairwise interaction potential $w(R)$ for a transferable model optimized at 300 K and the corresponding mean energy potential $\overline{u}(R)$. Qualitatively, the behavior of these functions is similar to the respective U_2 and E_2 given in Ref. 26. Comparing Fig. S7(d) showing entropy potentials with Fig. 4(a) of Ref. 26, the same kind of behavior is observed below 3 Å, although entropy potentials approximated by finite differences show a relatively consistent deviation from the model entropy potential compared to the highly oscillatory potentials seen in Ref. 26. Curiously, there is a quantitative difference between the interaction potentials that may arise from incomplete convergence of the IBI approach noted in Ref. 26 and the insensitivity of $g(R)$ to the potentials. We do not investigate the density dependence of our models here, but it is also worth noting that our density ρ = 998 kg/m^3 differs from the density ρ = 988 kg/m^3 of Ref. 26. The inner well in the energy potential E_2 of Ref. 26 is much deeper than the one seen here—this may be a consequence of the lack of one-body terms in the dual-potential approach used for water in Ref. 26. In a different study, Lebold and Noid[25] considered implicit solvent models using their approach and introduced an energy offset that, if applied for these SPC/E water models, would likely change the nature of the energy potential.

Although the authors of Ref. 25 studied different systems than the ones we consider here, they presented an interesting theoretical result that is instructive to compare with the results of our approach. There, the authors showed that energy fluctuations in a system can be decomposed into those due to the averaged behavior of CG sites and those occurring within the sites themselves; in our notation,

$$\sigma^2_{U_{\mathrm{AA}}} = \left\langle \left[U_{W_{\mathrm{AA}}}(\mathbf{R}^N) - \langle U_{\mathrm{AA}} \rangle_{\mathrm{AA}} \right]^2 \right\rangle_{\mathrm{AA}} + \left\langle \left[U_{\mathrm{AA}} - U_{W_{\mathrm{AA}}}(\mathbf{R}^N) \right]^2 \right\rangle_{\mathrm{AA}}. \tag{56}$$

The models in Ref. 26 can accurately predict mean energies, but energy fluctuations are consistently too small. This is a consequence of only capturing the pre-averaged behavior of the energy fluctuations, i.e., the first of the two ensemble averages in Eq. (56). In our CG models, this corresponds to fluctuations in $\overline{U}$, which can be seen in, e.g., Fig. 4(a) to be lower than those of U_{AA} in our models. However, the variance of E predicted by the models here is actually

$$\sigma^2_E = \sigma^2_{\overline{U}} + \langle \Gamma \rangle_{\mathrm{CG}} \tag{57}$$

(see the supplementary material, Sec. II F); the first term gives the averaged fluctuations, while the second re-introduces the atomistic fluctuations within CG sites that would normally be lost in coarse-graining. This comparison highlights the critical importance of capturing *all* the contributions to fluctuations in an AA system when trying to recover its energy distribution.

Overall, these results for SPC/E water are promising and suggest that even in small rigid molecules with few coarse-grained degrees of freedom (here, only orientational degrees of freedom), the microcanonical approach is still able to well-resolve the temperature dependence of configurational and energetic probability distributions. We have also conducted tests with the flexible but otherwise very similar SPC/Fw water model. The presence of intramolecular bonded fluctuations in this non-rigid model does not appear to influence the behaviors described above, including the tendency of the microcanonical approach to match pairwise forces in the inner attractive region of the potential. Results for this model, provided in Fig. S8, are almost identical to those for rigid SPC/E.

V. CONCLUSIONS

In this work, we proposed a new framework for the systematic development of temperature-transferable coarse-grained (CG) models. This approach is built upon two key ideas: that temperature-transferable CG models can be treated in a microcanonical manner

by considering configuration-dependent densities of states and that relative entropy provides a natural way to systematically optimize such models by extension to joint energy-configuration distributions. The theoretical framework underlying this approach is based on a rigorous decomposition of the CG free energy into energetic and entropic components. Energy fluctuations associated with degrees of freedom removed during coarse-graining, rather than being discarded entirely, are naturally encapsulated within microcanonical CG models and their predicted energy distributions. Contributions to CG energies are partitioned into standard two-body terms representing interactions between CG sites and additional one-body terms nominally representing degrees of freedom internal to individual sites. Overall, these models allow not only for accurate transferability but also for the unique ability to sample AA energy distributions for any given coarse configuration as well as the entire CG ensemble. The distributions themselves can also be transferred to new temperatures, addressing the combined representability and transferability problem as it pertains to temperature and energy.

Overall, our test results for model Lennard-Jones systems indicate that the approach is robust and able to accurately predict radial distribution functions and energy distributions over ranges of temperatures. Dodecane and water results confirm these findings on real systems. Handling of the one-body parameters necessary to match energy distributions can be performed in several ways; optimizing them alongside other parameters, or fixing them based on reference simulations, appears to give the best results. Future work exploring this approach and our implementation might investigate more numerically robust ways to parameterize this class of models, with attention to both optimal strategies for addressing the one-body terms as well as effective treatment for the poorly sampled inner-core region of pair potentials. Other questions related to the method include its relationship to other schemes for creating temperature-transferable models and their performance on different kinds of systems.

The termwise decomposition of the density of states along with the normal distribution approximation for the energies is motivated primarily by its mathematical convenience. Additionally, a Gaussian functional form for the overall CG density of states in Eq. (17) corresponds to a parabolic approximation to the CG configuration-dependent microcanonical entropy. Given that this function should be concave with respect to the energy, the normal approximation is especially natural since it acts as an expansion to second order, giving the simplest possible physically realistic functional form for the microcanonical entropy. For all the systems studied here, overall energy distributions were very accurately approximated to be normal. In theory, more complex or weakly coarse-grained systems involving interactions leading to highly non-Gaussian energy distributions, and strong correlations between degrees of freedom, could reach the limits of the assumptions made here. As the decomposition of the density of states into terms is quite general, other distribution forms such as the gamma distribution that models constant heat capacities could be used. More complex forms such as Gaussian mixture models might be applicable in theory, although the necessary convolutions would quickly become intractable for all but the simplest of models. We note that the random energy model for disordered systems,[91,92] which makes a similar normal energy approximation, has been used to study protein folding,[93,94] suggesting that such a model for energies can still be useful when applied to complex macromolecular systems.

The present method is also not limited to the pairwise nonbonded interactions and normal energy distributions that we consider here. For example, bonded potentials and other non-bonded multibody interactions such as local density potentials could be employed. More broadly, this work suggests a general strategy for addressing transferability issues by extending the relative entropy to add variables that augment the conventional configurational distribution. While here we illustrated the extension to the joint energy-configuration probability space (i.e., energy is added as a distribution variable), this conceptual approach suggests the potential for using additional fluctuating variables natural to other ensembles, such as volume in the isothermal–isobaric ensemble, as has been considered in the context of MS-CG.[18,37,41] In each case, the relative entropy formalism can then be used to determine a form for the appropriate partition function (or thermodynamic potential) relevant to the fluctuations of interest. The novel features of this approach make it a potentially productive strategy for overcoming the transferability problem in coarse-graining and ultimately for creating more powerful and useful multiscale models.

SUPPLEMENTARY MATERIAL

See the supplementary material for supplementary figures presenting additional data on transferable model performance, derivations of selected equations, and discussion of optimization of one-body parameters.

ACKNOWLEDGMENTS

We acknowledge funding support from the National Science Foundation through Award No. CHEM-1800344. This material is based on the work supported by the National Science Foundation Graduate Research Fellowship under Grant No. 1650114. Use was made of computational facilities purchased with funds from the National Science Foundation (Grant No. OAC-1925717) and administered by the Center for Scientific Computing (CSC). The CSC is supported by the California NanoSystems Institute and the Materials Research Science and Engineering Center (MRSEC, NSF Grant No. DMR 1720256) at UC Santa Barbara.

DATA AVAILABILITY

The data that support the findings of this study are available from the corresponding author upon reasonable request.

REFERENCES

[1] J. J. de Pablo, AIChE J. **51**, 2371 (2005).
[2] M. Praprotnik, L. D. Site, and K. Kremer, Annu. Rev. Phys. Chem. **59**, 545 (2008).
[3] P. Sherwood, B. R. Brooks, and M. S. P. Sansom, Curr. Opin. Struct. Biol. **18**, 630 (2008).
[4] S. Riniker, J. R. Allison, and W. F. van Gunsteren, Phys. Chem. Chem. Phys. **14**, 12423 (2012).
[5] A. J. Pak and G. A. Voth, Curr. Opin. Struct. Biol. **52**, 119 (2018).
[6] S. Y. Joshi and S. A. Deshmukh, Mol. Simul. **47**, 786 (2020).

[7]A. K. Soper, Chem. Phys. **202**, 295 (1996).
[8]D. Reith, M. Pütz, and F. Müller-Plathe, J. Comput. Chem. **24**, 1624 (2003).
[9]M. S. Shell, in *Advances in Chemical Physics*, edited by S. A. Rice and A. R. Dinner (John Wiley & Sons, Inc., Hoboken, NJ, 2016), Vol. 161, pp. 395–441.
[10]M. S. Shell, J. Chem. Phys. **129**, 144108 (2008).
[11]A. Chaimovich and M. S. Shell, J. Chem. Phys. **134**, 094112 (2011).
[12]S. Izvekov and G. A. Voth, J. Chem. Phys. **123**, 134105 (2005).
[13]S. Izvekov and G. A. Voth, J. Phys. Chem. B **109**, 2469 (2005).
[14]W. G. Noid, P. Liu, Y. Wang, J.-W. Chu, G. S. Ayton, S. Izvekov, H. C. Andersen, and G. A. Voth, J. Chem. Phys. **128**, 244115 (2008).
[15]W. G. Noid, J.-W. Chu, G. S. Ayton, V. Krishna, S. Izvekov, G. A. Voth, A. Das, and H. C. Andersen, J. Chem. Phys. **128**, 244114 (2008).
[16]A. Chaimovich and M. S. Shell, Phys. Rev. E **81**, 060104 (2010).
[17]T. T. Foley, M. S. Shell, and W. G. Noid, J. Chem. Phys. **143**, 243104 (2015).
[18]N. J. H. Dunn, T. T. Foley, and W. G. Noid, Acc. Chem. Res. **49**, 2832 (2016).
[19]D. Rosenberger and N. F. A. van der Vegt, Phys. Chem. Chem. Phys. **20**, 6617 (2018).
[20]J. Jin, A. J. Pak, and G. A. Voth, J. Phys. Chem. Lett. **10**, 4549 (2019).
[21]J. W. Mullinax and W. G. Noid, J. Chem. Phys. **131**, 104110 (2009).
[22]T. Sanyal and M. S. Shell, J. Chem. Phys. **145**, 034109 (2016).
[23]J. W. Wagner, T. Dannenhoffer-Lafage, J. Jin, and G. A. Voth, J. Chem. Phys. **147**, 044113 (2017).
[24]V. Krishna, W. G. Noid, and G. A. Voth, J. Chem. Phys. **131**, 024103 (2009).
[25]K. M. Lebold and W. G. Noid, J. Chem. Phys. **151**, 164113 (2019).
[26]K. M. Lebold and W. G. Noid, J. Chem. Phys. **150**, 234107 (2019).
[27]J. G. Kirkwood, J. Chem. Phys. **3**, 300 (1935).
[28]A. P. Lyubartsev and A. Laaksonen, Phys. Rev. E **52**, 3730 (1995).
[29]J. F. Rudzinski and W. G. Noid, J. Phys. Chem. B **116**, 8621 (2012).
[30]A. P. Lyubartsev, A. Naômé, D. P. Vercauteren, and A. Laaksonen, J. Chem. Phys. **143**, 243120 (2015).
[31]A. A. Louis, J. Phys.: Condens. Matter **14**, 9187 (2002).
[32]R. Halder and B. Jana, J. Phys. Chem. B **122**, 6801 (2018).
[33]P. Ganguly, D. Mukherji, C. Junghans, and N. F. A. van der Vegt, J. Chem. Theory Comput. **8**, 1802 (2012).
[34]P. Ganguly and N. F. A. van der Vegt, J. Chem. Theory Comput. **9**, 5247 (2013).
[35]T. C. Moore, C. R. Iacovella, and C. McCabe, J. Chem. Phys. **140**, 224104 (2014).
[36]T. D. Potter, J. Tasche, and M. R. Wilson, Phys. Chem. Chem. Phys. **21**, 1912 (2019).
[37]N. J. H. Dunn and W. G. Noid, J. Chem. Phys. **144**, 204124 (2016).
[38]L. Larini, L. Lu, and G. A. Voth, J. Chem. Phys. **132**, 164107 (2010).
[39]A. Das and H. C. Andersen, J. Chem. Phys. **136**, 194114 (2012).
[40]S. Izvekov, P. W. Chung, and B. M. Rice, J. Chem. Phys. **133**, 064109 (2010).
[41]A. Das and H. C. Andersen, J. Chem. Phys. **132**, 164106 (2010).
[42]N. J. H. Dunn and W. G. Noid, J. Chem. Phys. **143**, 243148 (2015).
[43]P. Vanya and J. A. Elliott, Phys. Rev. E **102**, 013312 (2020).
[44]T. Sanyal and M. S. Shell, J. Phys. Chem. B **122**, 5678 (2018).
[45]M. R. DeLyser and W. G. Noid, J. Chem. Phys. **147**, 134111 (2017).
[46]M. DeLyser and W. G. Noid, J. Chem. Phys. **153**, 224103 (2020).
[47]M. R. DeLyser and W. G. Noid, J. Chem. Phys. **151**, 224106 (2019).
[48]E. C. Allen and G. C. Rutledge, J. Chem. Phys. **128**, 154115 (2008).
[49]E. C. Allen and G. C. Rutledge, J. Chem. Phys. **130**, 034904 (2009).
[50]J. Ghosh and R. Faller, Mol. Simul. **33**, 759 (2007).
[51]P. Carbone, H. A. K. Varzaneh, X. Chen, and F. Müller-Plathe, J. Chem. Phys. **128**, 064904 (2008).
[52]K. Farah, A. C. Fogarty, M. C. Böhm, and F. Müller-Plathe, Phys. Chem. Chem. Phys. **13**, 2894 (2011).
[53]K. M. Lebold and W. G. Noid, J. Chem. Phys. **150**, 014104 (2019).
[54]M. Z. Griffiths and W. Shinoda, J. Chem. Inf. Model. **59**, 3829 (2019).
[55]J. Ruza, W. Wang, D. Schwalbe-Koda, S. Axelrod, W. H. Harris, and R. Gómez-Bombarelli, J. Chem. Phys. **153**, 164501 (2020).
[56]G. Deichmann, M. Dallavalle, D. Rosenberger, and N. F. A. van der Vegt, J. Phys. Chem. B **123**, 504 (2019).
[57]J. Jin, A. Yu, and G. A. Voth, J. Chem. Theory Comput. **16**, 6823 (2020).
[58]W. Xia, J. Song, C. Jeong, D. D. Hsu, F. R. Phelan, J. F. Douglas, and S. Keten, Macromolecules **50**, 8787 (2017).
[59]S. Jephthah, L. Staby, B. B. Kragelund, and M. Skepö, J. Chem. Theory Comput. **15**, 2672 (2019).
[60]L. Lu and G. A. Voth, J. Chem. Phys. **134**, 224107 (2011).
[61]G. Tóth, J. Phys.: Condens. Matter **19**, 335222 (2007).
[62]J. I. Monroe, H. W. Hatch, N. A. Mahynski, M. S. Shell, and V. K. Shen, J. Chem. Phys. **153**, 144101 (2020).
[63]T. Bereau and J. F. Rudzinski, Phys. Rev. Lett. **121**, 256002 (2018).
[64]J. F. Rudzinski and T. Bereau, J. Chem. Phys. **153**, 214110 (2020).
[65]J. F. Dama, A. V. Sinitskiy, M. McCullagh, J. Weare, B. Roux, A. R. Dinner, and G. A. Voth, J. Chem. Theory Comput. **9**, 2466 (2013).
[66]A. Davtyan, J. F. Dama, A. V. Sinitskiy, and G. A. Voth, J. Chem. Theory Comput. **10**, 5265 (2014).
[67]H.-J. Qian, P. Carbone, X. Chen, H. A. Karimi-Varzaneh, C. C. Liew, and F. Müller-Plathe, Macromolecules **41**, 9919 (2008).
[68]D. D. Hsu, W. Xia, S. G. Arturo, and S. Keten, Macromolecules **48**, 3057 (2015).
[69]H. Huang, L. Wu, H. Xiong, and H. Sun, Macromolecules **52**, 249 (2019).
[70]S. P. Carmichael and M. S. Shell, J. Phys. Chem. B **116**, 8383 (2012).
[71]P. Español, M. Serrano, I. Pagonabarraga, and I. Zúñiga, Soft Matter **12**, 4821 (2016).
[72]G. Faure, R. Delgado-Buscalioni, and P. Español, J. Chem. Phys. **146**, 224106 (2017).
[73]A. Chaimovich and M. S. Shell, Phys. Chem. Chem. Phys. **11**, 1901 (2009).
[74]J. F. Dama, J. Jin, and G. A. Voth, J. Chem. Theory Comput. **13**, 1010 (2017).
[75]S. Plimpton, J. Comput. Phys. **117**, 1 (1995).
[76]M. G. Martin and J. I. Siepmann, J. Phys. Chem. B **102**, 2569 (1998).
[77]P. Eastman, J. Swails, J. D. Chodera, R. T. McGibbon, Y. Zhao, K. A. Beauchamp, L.-P. Wang, A. C. Simmonett, M. P. Harrigan, C. D. Stern, R. P. Wiewiora, B. R. Brooks, and V. S. Pande, PLoS Comput. Biol. **13**, e1005659 (2017).
[78]H. J. C. Berendsen, J. R. Grigera, and T. P. Straatsma, J. Phys. Chem. **91**, 6269 (1987).
[79]Y. Wu, H. L. Tepper, and G. A. Voth, J. Chem. Phys. **124**, 024503 (2006).
[80]R. L. Henderson, Phys. Lett. A **49**, 197 (1974).
[81]H. Wang, F. H. Stillinger, and S. Torquato, J. Chem. Phys. **153**, 124106 (2020).
[82]F. H. Stillinger and T. Head-Gordon, Phys. Rev. E **47**, 2484 (1993).
[83]S. Garde and H. S. Ashbaugh, J. Chem. Phys. **115**, 977 (2001).
[84]M. E. Johnson, T. Head-Gordon, and A. A. Louis, J. Chem. Phys. **126**, 144509 (2007).
[85]H. Wang, C. Junghans, and K. Kremer, Eur. Phys. J. E **28**, 221 (2009).
[86]S. Y. Mashayak, L. Miao, and N. R. Aluru, J. Chem. Phys. **148**, 214105 (2018).
[87]J. Jin, Y. Han, A. J. Pak, and G. A. Voth, J. Chem. Phys. **154**, 044104 (2021).
[88]J. Jin, A. J. Pak, Y. Han, and G. A. Voth, J. Chem. Phys. **154**, 044105 (2021).
[89]J. D. Weeks, D. Chandler, and H. C. Andersen, J. Chem. Phys. **54**, 5237 (1971).
[90]J. F. Rudzinski and W. G. Noid, J. Chem. Phys. **135**, 214101 (2011).
[91]B. Derrida, Phys. Rev. Lett. **45**, 79 (1980).
[92]B. Derrida, Phys. Rev. B **24**, 2613 (1981).
[93]J. D. Bryngelson and P. G. Wolynes, J. Phys. Chem. **93**, 6902 (1989).
[94]V. S. Pande, A. Y. Grosberg, and T. Tanaka, Biophys. J. **73**, 3192 (1997).